frontiers | Frontiers in Cell and Developmental Biology

TYPE Original Research
PUBLISHED 31 October 2023
DOI 10.3389/fcell.2023.1144936

OPEN ACCESS

EDITED BY
Marcus Tindall,
University of Reading, United Kingdom

REVIEWED BY
Stéphanie Lebreton,
Institute Pasteur, France
Steven Watterson,
Ulster University, United Kingdom

*CORRESPONDENCE
Daniel Wüstner,
wuestner@bmb.sdu.dk

RECEIVED 15 January 2023
ACCEPTED 20 October 2023
PUBLISHED 31 October 2023

CITATION
Wüstner D, Dupont Juhl A, Egebjerg JM, Werner S, McNally J and Schneider G (2023), Kinetic modelling of sterol transport between plasma membrane and endo-lysosomes based on quantitative fluorescence and X-ray imaging data.
Front. Cell Dev. Biol. 11:1144936.
doi: 10.3389/fcell.2023.1144936

Kinetic modelling of sterol transport between plasma membrane and endo-lysosomes based on quantitative fluorescence and X-ray imaging data

Daniel Wüstner[1]*, Alice Dupont Juhl[1], Jacob Marcus Egebjerg[1], Stephan Werner[2], James McNally[2] and Gerd Schneider[2]

[1]Department of Biochemistry and Molecular Biology, University of Southern Denmark, Odense, Denmark, [2]Department of X-Ray Microscopy, Helmholtz-Zentrum Berlin, Berlin, Germany

Niemann Pick type C1 and C2 (NPC1 and NPC2) are two sterol-binding proteins which, together, orchestrate cholesterol transport through late endosomes and lysosomes (LE/LYSs). NPC2 can facilitate sterol exchange between model membranes severalfold, but how this is connected to its function in cells is poorly understood. Using fluorescent analogs of cholesterol and quantitative fluorescence microscopy, we have recently measured the transport kinetics of sterol between plasma membrane (PM), recycling endosomes (REs) and LE/LYSs in control and NPC2 deficient fibroblasts. Here, we use kinetic modeling of this data to determine rate constants for sterol transport between intracellular compartments. Our model predicts that sterol is trapped in intraluminal vesicles (ILVs) of LE/LYSs in the absence of NPC2, causing delayed sterol export from LE/LYSs in NPC2 deficient fibroblasts. Using soft X-ray tomography, we confirm, that LE/LYSs of NPC2 deficient cells but not of control cells contain enlarged, carbon-rich intraluminal vesicular structures, supporting our model prediction of lipid accumulation in ILVs. By including sterol export via exocytosis of ILVs as exosomes and by release of vesicles—ectosomes—from the PM, we can reconcile measured sterol efflux kinetics and show that both pathways can be reciprocally regulated by the intraluminal sterol transfer activity of NPC2 inside LE/LYSs. Our results thereby connect the *in vitro* function of NPC2 as sterol transfer protein between membranes with its *in vivo* function.

KEYWORDS

sterol, diffusion, kinetic modelling, Niemann-Pick disease type C2, differential equations, time-delay, X-ray microscopy, cholesterol efflux

1 Introduction

Late endosomes and lysosomes (LE/LYSs) play important roles in degradation of biomolecules and in sensing the nutritional status of the cell (Appelqvist et al., 2013; Settembre et al., 2013). To exert such functions, the abundance of cholesterol and other lipids in the limiting membrane as well as in internal vesicles of LE/LYSs is crucial (Chevallier et al.,

2008). Lysosomal cholesterol accumulation impairs membrane fusion and luminal acidification, attenuates cellular death pathways and affects virus entry and replication (Cox et al., 2007; Fraldi et al., 2010; Appelqvist et al., 2011; Carette et al., 2011; Stoeck et al., 2018). Mammalian cells receive most of their cholesterol from receptor-mediated endocytosis of low density lipoprotein (LDL), which dissociates from its receptor in early endosomes followed by trafficking of LDL to LE/LYSs for degradation (Goldstein and Brown, 2009; Luo et al., 2020). Regulation of this trafficking pathway is complex and ensures sufficient cholesterol supply but also prevention of cholesterol accumulation (Goldstein et al., 2006; Juhl and Wüstner, 2022).

Several proteins have been involved in export of endogenous and LDL derived cholesterol from LE/LYSs (Luo et al., 2020; Juhl and Wüstner, 2022; Lu, 2022). Among them, Niemann Pick C1 and C2 (NPC1 and NPC2) play a central role, and mutations in either protein can lead to pronounced accumulation of cholesterol and other lipids in LE/LYSs of various organs, including the brain—a hallmark of Niemann Pick type C disease. NPC1 is a large transmembrane protein in the limiting membrane of endo-lysosomes with at least two sterol binding sites; one in the luminal N-terminal domain (NTD) and the other in the transmembrane sterol sensing domain (SSD), respectively (Pfeffer, 2019). NPC2 is a small sterol-binding protein in the lumen of LE/LYSs which has been shown to facilitate sterol exchange between model membranes (Xu et al., 2008; McCauliff et al., 2011). Mammalian and yeast NPC2 can transfer sterol to the NTD of NPC1 (named NCR1 in yeast), suggesting a mechanism for sterol transfer between both proteins in the LE/LYSs (Infante et al., 2008; Wang et al., 2010; Winkler et al., 2019). NPC2 has been shown to bind to NPC1 but also to other abundant proteins in endo-lysosomes, such as LAMP-2, suggesting that NPC2 functions as a sterol donor to various membrane proteins in the lysosomal membrane (Deffieu and Pfeffer, 2011; Li et al., 2016; Li and Pfeffer, 2016).

There have been several attempts to model the transport defects observed in human fibroblasts lacking functional NPC1; Neufeld and co-workers used compartment modeling to predict impaired recycling from a late endosomal compartment back to the PM in NPC1 deficient cells (Neufeld et al., 1999). Lange and Steck compared cholesterol transport in fibroblasts from healthy subjects and NPC1 disease patients using cholesterol isotopes and subcellular fractionation (Lange et al., 1998). They proposed a simple kinetic model to explain their data in which they assumed that cholesterol exchanges bi-directionally between the PM and the LE/LYSs (Lange et al., 1998). This model was based on studies with radioactive cholesterol which provided evidence for recycling of PM-derived sterol from LE/LYSs (Lange et al., 1997; Lange et al., 2000; Lange et al., 2002). They found that the rate constant describing transport from the PM to LE/LYS ($k_{PM \rightarrow LE/LYS}$) is increased in NPC1 disease compared to control cells, while the transport in the opposite direction (i.e., from the LE/LYS to the PM; $k_{LE/LYS \rightarrow PM}$) is slowed down. Together, this resulted in a 2-3-fold expanded sterol pool in the NPC1 disease cells at steady state, with no change in the ER pool size (Lange et al., 1998). In an attempt to test this model for NPC2-deficient cells, we used live-cell imaging of the cholesterol analog DHE and found evidence for impaired sterol export from LE/LYSs back to the PM but not for enhanced sterol endocytosis (Berzina et al., 2018). DHE is intrinsically fluorescent with no dye molecule attached to it and therefore resembles cholesterol very closely. It has been shown in several cell lines that DHE and similar sterol probes are initially transported from the PM to early endosomes comprised of sorting endosomes and the endocytic recycling compartment, here abbreviated as recycling endosomes (REs) (Hao et al., 2002; Wüstner et al., 2002; Wüstner et al., 2005; Petersen et al., 2008). Sterol trafficking to REs has not been included in the model presented previously by Lange and co-workers, which only considered bi-directional sterol exchange between PM and LE/LYS (Lange et al., 1998). REs are cholesterol-rich organelles, and they ensure efficient recycling of proteins, such as transferrin and its receptor. Endocytic recycling takes place in two circuits, fast recycling from peripheral sorting endosomes and slower recycling from a perinuclear endocytic recycling compartment [reviewed in Maxfield and Mcgraw (2004)]. We found that DHE is rapidly transported from the PM to REs in human fibroblasts, irrespective of whether functional NPC2 is expressed in those cells or not (Berzina et al., 2018).

In NPC2-deficient fibroblasts, we found that DHE became trapped in LE/LYSs, and that the endo-lysosomes move slower compared to fibroblasts from healthy subjects (Lund et al., 2014; Berzina et al., 2018). Incubating disease cells with purified NPC2 rescued the lysosomal sterol storage phenotype and increased directional movement of LE/LYS towards the PM, from where the excess sterol was released (Lund et al., 2014; Juhl et al., 2021b). We also showed that this last step is facilitated by ABCA1/Apoprotein A1 and involves shedding of sterol-rich vesicles from the PM (Juhl et al., 2021b). While we could demonstrate that internalized NPC2 co-localizes extensively with fluorescent cholesterol analogues during efflux, we do not know, exactly how it could activate the trapped sterol pool inside LE/LYSs. To answer this question, we combine here mathematical modeling of the previously published sterol transport data with X-ray microscopy of the ultrastructure of endo-lysosomes of control and NPC2-deficient cells. Our modelling analysis and experimental results can explain the observed defects in intracellular sterol transport and efflux in NPC2-deficient cells as a consequence of impaired sterol transfer from ILVs to the limiting membrane of LE/LYSs. This leads to an expansion of the sterol pool in ILVs which can be released from cells as exosomes by lysosomal exocytosis. Our model analysis shows that this sterol efflux pathway could dominate in NPC2-deficient cells, while in control cells, the more efficient delivery of sterol to the PM allows for preferred sterol efflux from the cell surface. Efflux of cholesterol from the PM could be mediated by release of vesicles, so-called ectosomes, as well as by extracellular acceptor proteins, like apoprotein A1 (apoA1) and albumin. Our study provides an integrated model combining the established *in-vitro* function of NPC2 as sterol transfer protein and lipid solubilizer with its *in vivo* function in regulating cholesterol flux from endo-lysosomes.

2 Methods

2.1 Reagents, cell culture and labeling for fluorescence and X-ray microscopy

Human skin fibroblasts from control subject (Coriell Institute #GM08680) were from a male healthy donor, while NPC2 deficient

human skin fibroblasts were from Coriell Institute #GM18455 (a male patient affected by two point mutations at the NPC2 locus resulting in a nonsense mutation at codon 20 in allele 1 and in a missense mutation at codon 47 of allele 2, respectively). They were grown at 37°C in an atmosphere of 5% CO_2 until 90% confluence in complete DMEM culture medium (from GIBCO BRL; Life Technologies, Paisley, Scotland) supplemented with 1% glutamine, 1% penicillin and 20% FBS for diseased cells or 10% FBS for control cells. In some experiments, 100 nM NPC2 (purified from bovine milk as described previously and kindly provided by Dr. Christian Heegaard from Aarhus university (Berzina et al., 2018)) was added in human lipoprotein depleted serum (LPDS) for 48 h. TopFluor-cholesterol (TF-Chol), LPDS and other reagents were from SIGMA (Denmark). Buffer medium contained 150 mM NaCl, 5 mM KCl, 1 mM CaCl2, 1 mM MgCl2, 5 mM glucose and 20 mM HEPES (pH 7.4). TF-Chol was loaded onto methyl-β-Cyclodextrin to form a complex as described (Juhl et al., 2021b). Briefly, 1.5 μM of TF-Chol from an ethanol stock were dried under nitrogen and mixed with phosphate buffer solution (PBS) containing 1 mg BSA and 40 mg MCD to a final volume of 2 mL under rigorous vortexing for 5 min. Cells were washed with buffer medium before they were pulse labeled for 3 min with 100 μL TF-Chol/MCD solution, washed and chased for 2 h at 37°C, in buffer medium followed by fixation in 4% paraformaldehyde (PFA) and imaging as described (Juhl et al., 2021b). For DHE efflux experiments, the sterol was loaded onto albumin, as described previously (Juhl et al., 2021b). Cells were incubated with DHE/albumin solution overnight in the presence of 0.5 mg/mL rhodamine labeled dextran (Rh-dextran; 70 kD purchased from Invitrogen, Waltham, MA, United States), followed by washing and incubation in culture medium with LPDS but without sterol source for varying times. For imaging, cells were washed with buffer medium and imaged on a Leica DMIRB wide field microscope with 100x, NA1.4 objective with high UV transmission. DHE was imaged using a filter cube with a 335 nm (20 nm bandpass) excitation filter, 365 nm dichromatic mirror and 405 nm (40 nm bandpass) emission filter on the Leica DMIRB microscope as described (Juhl et al., 2021b). For imaging of Rh-dextran a standard rhodamine filter set with a 535 nm (50 nm bandpass) excitation filter, 565 nm dichromatic mirror and 610 nm (75 nm bandpass) emission filter was used.

2.2 Generation of fluorescence time courses as input for modeling, data regression and calculations

Fractional fluorescence of the cholesterol analog DHE in the PM, REs and LE/LYSs was measured in fibroblasts from healthy subjects or from NPC2 disease patients, as described in our previous publication (Berzina et al., 2018). Quantification was based on image segmentation using organelle-specific markers and the ImageJ program with an in-house developed plugin (Rueden et al., 2017; Berzina et al., 2018). Briefly, in pulse-chase experiments, cells were pre-labeled with Rh-dextran, a marker for LE/LYSs, overnight, washed, labeled with DHE/MCD for 3 min, washed and chased for various times. REs were stained with Alexa647-tagged transferrin during the last 20 min of incubation. Measurement of DHE transport kinetics from these experiments is briefly described in Supplementary Figure S1 with further detail in Berzina et al. (2018). In continuous-uptake experiments, cells were incubated with DHE/albumin in the presence of Rh-dextran, as described above. For multi-compartment parameter estimation global optimization routines either implemented in the SAAM software or in the Symfit python module were used (Barrett et al., 1998). Steady states of the dynamic system and the differential equation for the Weibull model were calculated using Mathematica (Wolfram Research Inc., United States) or SymPy, a python library for symbolic calculations (Meurer et al., 2017). Numeric simulations of the ordinary differential equation systems that we derived were implemented either in Mathematica or in Python using the odeint module of SciPy (Virtanen et al., 2020).

2.3 Soft X-ray tomography of human fibroblasts

Healthy and NPC2 deficient human fibroblasts were grown to a confluency of 90%, and, after trypsin treatment, split onto Poly-D-Lysine coated R 2/2 grids (QUANTIFOIL 100 Holey Carbon Films, Grids: HZB-2 Au), which were fixed to the bottom of 12 well plates. Cells were allowed to settle for another 48–72 h before further treatment and fixed with 4% PFA. The cells were kept in 1xPBS until cryo-plunge freezing with liquid ethane and subsequently stored and imaged under liquid nitrogen temperature. Prior to the plunge freezing, a small volume of ~270 nm silica beads with an outer gold shelf were added to the samples, to serve as fiducial markers for tomographic reconstruction. Soft X-ray tomography (SXT) was performed at Bessy II electron storage ring at the Helmholtz Zentrum Berlin. The SXT data was collected at the full-field transmission X-ray microscope at the beamline U41-PGM, with an X-ray energy of 510 eV and a 25 nm zone plate. Cells were kept under liquid nitrogen temperature during imaging and imaged over a range of 120-125° tilt angels with 1° step size. To collect the fluorescent signal, a widefield microscope connected to the X-ray microscope, with an ×100 objective, NA = 0.7, was used. The image pixel size was 9.8 nm for SXT and 148 nm for fluorescence microscopy. For alignment of tomogram frames, B-soft was used, while the Tomo3D software was used for reconstructions based on the filtered back-projection algorithm (Heymann and Belnap, 2007; Agulleiro and Fernandez, 2015). Sum projections of selected frames along the reconstructed 3D stack were calculated with in-house developed Macro scripts to ImageJ [Macro Language (nih.gov)]. Registration of fluorescence and X-ray images was done in Icy using the ec-CLEM plugin with 3-5 image points as reference markers [ec-CLEM |—Open Source Image Processing Software (bioimageanalysis.org)].

2.4 Four-compartment model of sterol transport

Mathematically, any compartment system with time lags can be adequately described by assuming one or several intermediate compartments (which is sometimes called the 'linear chain trick') (Jacquez and Simon, 2002). The mathematical model, we present

here, combines observations on lysosomal sterol trafficking from the literature with our published data by considering sterol transport from the PM (with sterol amount n_1) to the REs (with sterol amount n_2) and further to LE/LYSs (with sterol amount n_3) and from there back to the PM (Berzina et al., 2018). Importantly, transport between PM, REs and LE/LYSs is modeled as unidirectional in our model, which simplifies the parametrization significantly. Still, the overall transport between PM and LE/LYS is reversible, accounting for the experimentally observed sterol cycling. The system of ordinary differential equations (ODE) describing the whole model is given by

$$\frac{dn_1}{dt} = -k_1 \cdot n_1 + k_3 \cdot n_3 \tag{1a}$$

$$\frac{dn_2}{dt} = k_1 \cdot n_1 - k_2 \cdot n_2 \tag{1b}$$

$$\frac{dn_3}{dt} = k_2 \cdot n_2 - (k_3 + k_4) \cdot n_3 + k_{-4} \cdot n_4 \tag{1c}$$

$$\frac{dn_4}{dt} = k_4 \cdot n_3 - k_{-4} \cdot n_4 \tag{1d}$$

The amount of sterol in the ith compartment is given by n_i (with $i = 1, \ldots, 4$), and it is assumed that the abundance of DHE in each membrane compartment is proportional to the integrated fluorescence intensity in this compartment. Thus, we directly modelled the fluorescence time courses without conversion into concentration units for which one would need to know the exact compartment volumes. Since those volumes are very difficult to obtain from fluorescence micrographs and because the rate constants, we aimed to infer from our model are first order (i.e., with units of per sec), this option has been neglected. The ODE system in Eqs 1a–1d was solved numerically and the model solutions were fitted to the experimental time courses by a global non-linear regression implemented in SAAM (SAAM Institute, Seattle, WA, United States), as described previously (Wüstner, 2005b). That means parameter sets are determined in parallel from all experimental time courses for control and disease fibroblasts, respectively. In some earlier applications of this approach, we showed that global fitting using SAAM provides high reliability in the fitting performance (Wüstner, 2005a; Wüstner, 2005b; Wüstner, 2006a; Wüstner, 2006b). Since we cannot distinguish between the sub-compartments of LE/LYSs in our experiments, the numerical solutions of Eqs 1c, 1d (i.e., for $n_3(t)$ and $n_4(t)$) were combined, and this sum was fitted to the time dependent DHE fraction in LE/LYSs.

Incorporating sterol uptake and release from the PM into the model leads to a new equation for the PM pool (replacing Eq.1a) according to (Figure 2A):

$$\frac{dn_1}{dt} = v_0 - (k_1 + k_5) \cdot n_1 + k_3 \cdot n_3 \tag{2}$$

Here, v_0 is the constant rate of sterol uptake, which can be seen as product of a rate constant, k_0, times a constant sterol amount, n_0, bound to albumin in the extracellular reservoir (i.e., $v_0 = k_0 \cdot n_0$). Since we consider this extracellular sterol pool to be in large excess of all cell-associated DHE, the influx v_0 is taken to be a constant. Sterol release from the PM, on the other hand, is proportional to the sterol abundance in the PM with the rate constant k_5 as proportionality constant. Importantly, continuous sterol uptake and release ensures that the studied cellular system becomes a thermodynamically open system with constant in- and outflow. This allows us to calculate a steady state fraction of sterol in each compartment (see Supplementary Materials).

3 Results

3.1 A four-compartment model of sterol transport reconciles defects in NPC2-deficient cells

Here, we attempted to extend the model developed by Lange & Steck to include transport through REs and also to account for the observation, that sterol efflux from cells is often found to be biphasic suggesting some type of compartmental system with lags for sterol efflux (Haynes et al., 2000; Hao et al., 2002). Similar to Lange & Steck, we model also sterol cycling between PM and LE/LYSs but consider REs as an intermediate compartment. We did not include several other compartments in our model because current data indicates they contribute only a small amount to sterol exchange with the PM. Specifically, we do not consider the ER sterol pool nor sterol esters, since only very little sterol is transported from the PM to acyl-coenzyme A acyl transferase (ACAT) in the ER in our experiments (i.e., about 1.5% of total DHE and ca. 6% and 0.4% of internalized radioactive cholesterol in control and disease cells, respectively, as judged by lipidomics analysis of sterol esterification) (Berzina et al., 2018). While this sterol pool is important for regulation of cholesterol synthesis and for expression of sterol transporters (Infante and Radhakrishnan, 2017), it is not quantitatively relevant in the context of our analysis. Also, the trafficking route of some sterol to the trans-Golgi network (TGN) is not considered in our model, as we did not observe significant enrichment of PM-derived DHE in the TGN in our experiments in human fibroblasts or other cell types (Hao et al., 2002; Wüstner et al., 2002; Wüstner et al., 2005; Berzina et al., 2018). A minor portion of sterol also reaches mitochondria in an NPC2 dependent manner, and we were able to visualize this pool in our recent study using live-cell imaging of cholestatrienol (CTL), another close fluorescent analog of cholesterol (Juhl et al., 2021a). However, the cholesterol content of mitochondria is very low, in part due to its rapid conversion to oxysterols in fibroblasts (Lange et al., 2009). Supporting this notion, we found only faint labeling of mitochondria with CTL derived from the PM, and even though this transport depends on NPC2, it does not contribute significantly to the total sterol flux between the PM and endo-lysosomes (Juhl et al., 2021a). It was therefore not included in our model, which is shown in Figure 1A and explained in section 2., with PM and REs as compartment 1 and 2, respectively. All sterol tracer, here assumed to be the fluorescent cholesterol analogue DHE, is initially inserted only in the PM, which is ensured by a short pulse-labeling of human fibroblasts with DHE loaded onto cyclodextrin (Berzina et al., 2018). After washing cells, the transport kinetics of DHE to REs labeled with fluorescent transferrin and of LE/LYSs, stained with fluorescent dextran, is followed over time (Berzina et al., 2018). To describe the observed transport kinetics of DHE in cells lacking functional NPC2, we consider the LE/LYSs as being sub-compartmentalized into compartments 3 and 4, resembling the limiting endo-lysosomal membrane and the ILVs, respectively (Figure 1A). The need for

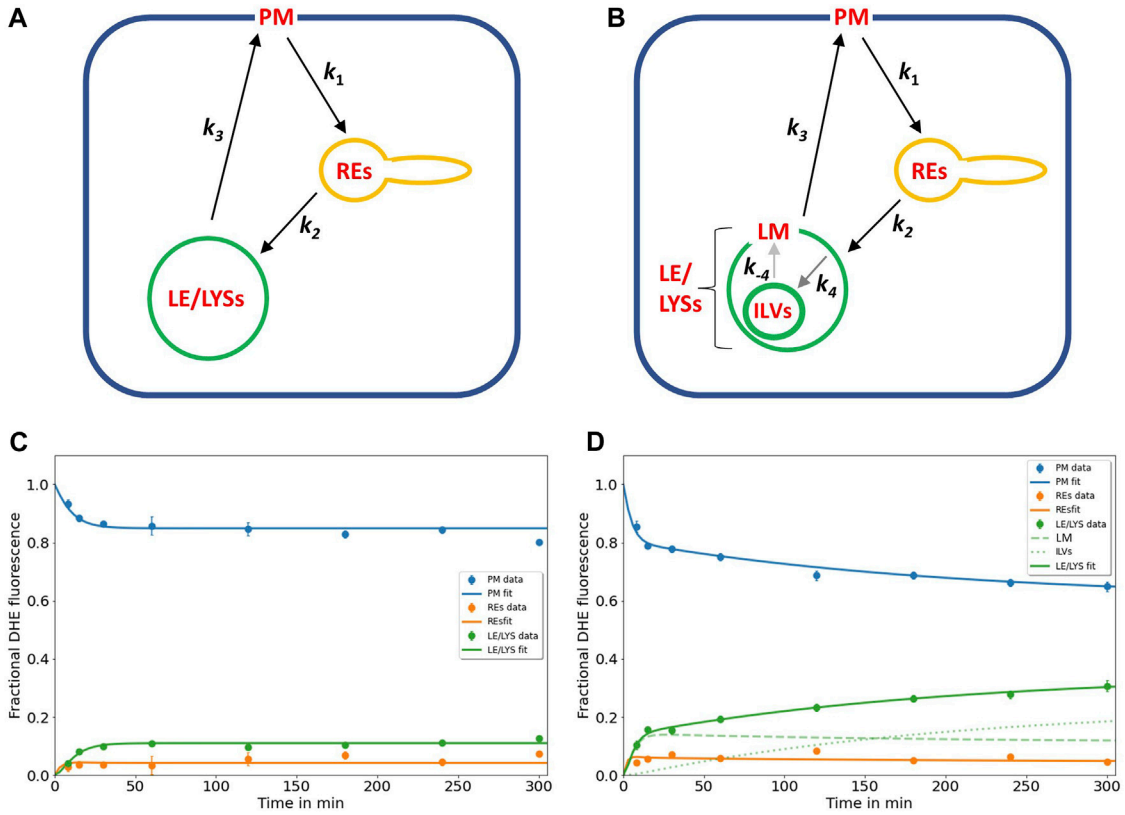

FIGURE 1
Kinetic modelling of sterol circulation between plasma membrane and LE/LYSs. **(A)**, sketch of the model describing sterol transport in control cells with sterol circulation between plasma membrane (PM; compartment 1), the recycling endosomes (REs; compartment 2) and late endosomes/lysosomes (LE/LYSs; compartment 3). The compartments are connected as indicated by the arrows, and sterol transport between them is parametrized by the given rate constants. **(B)**, to model the pulse-chase data for disease cells, the LE/LYSs must be subdivided into the lysosomal-membrane (LM, compartment 3) and intraluminal vesicles (ILVs, compartment 4), as otherwise the bi-phasic sterol accumulation in LE/LYSs cannot be explained, **(B)**. Sterol exchange between the third and fourth compartment is bi-directional (with rate constants k_4 and k_{-4}, respectively), but experimentally, we can only assess the sum of both compartments as LE/LYSs. In disease fibroblasts, the bidirectional exchange between limiting membrane and internal vesicles of LE/LYSs is assumed to be very slow due to lack of a functional NPC2 protein (grey arrows between LM and ILVs in B). C, D, fitting of the models to the experimental time courses of DHE transport in control cells **(C)** and disease cells **(D)**, respectively. The data was generated in our previous publication (Berzina et al., 2018). Results are shown for DHE in the PM (blue symbols, data; blue line, fit), for REs (orange symbols data; orange line, fit) and for LE/LYSs (green symbols, data; green straight line fit). For disease cells, LE/LYSs are modelled as sub-compartmentalized into limiting membrane (LM, compartment 3; green dashed line in D and thin green line in B) and ILVs (green dotted line in D and thick green line in B). See text for further information and Table 1 for derived parameters.

including a fourth compartment arose from the fact that the observed accumulation of DHE in LE/LYSs consists of two clearly separable phases in the disease cells (see Figure 1D, green circles). ILVs fulfil diverse functions in endosome maturation, protein degradation and lipid metabolism, and they are the precursor of secreted vesicles called exosomes [reviewed in Huotari and Helenius (2011)]. ILVs can be enriched in cholesterol, as shown by immunoelectron microscopy of sterol-binding perifringolysin derivatives (Möbius et al., 2002; Möbius et al., 2003). Also, *in vitro* evidence strongly support the hypothesis that NPC2 shuttles sterols between ILVs and the limiting membrane of LE/LYSs either to NPC1 or eventually bypassing NPC1 in the lysosomal membrane (Cheruku et al., 2006; Wang et al., 2010). Based on all these observations, we suggest that NPC2 regulates sterol exchange between compartment 3 (limiting membrane of LE/LYSs) and compartment 4 (ILVs). Absence of NPC2 leads to a biphasic increase of DHE in endo-lysosomes due to accumulation of the sterol in ILVs. Two kinetically defined sterol pools could in principle also relate to separate subpopulations of LE/LYSs (Goldman and Krise, 2010; van der Kant et al., 2013). However, our co-localization studies do not indicate that, as we found DHE enriched in all acidic endosomes in disease fibroblasts (Berzina et al., 2018).

Our model assumes well-mixed compartments, i.e., a homogeneous sterol distribution within each compartment due to rapid mixing of sterol entering each pool with sterol in that compartment. Thus, we exclude phase separation or slow mixing of either cholesterol or DHE in a given compartment This implies that DHE rapidly mixes with endogenous cholesterol pools, which is justified by the very similar biophysical properties of DHE and cholesterol; for example, DHE partitions into lipid domains similarly to cholesterol with strong preference for the liquid ordered phase in model membranes (Garvik et al., 2009). DHE also shows comparable interbilayer transfer rates to cholesterol, although DHE is slightly faster, and both sterols have similar lipid affinities, suggesting that they partition equally into different lipid

pools (Estronca et al., 2007). Also, transfer of both sterols is similarly accelerated by NPC2 protein, and DHE binds to a variety of intracellular sterol transfer proteins with similar affinity as cholesterol (Xu et al., 2008; Wüstner and Solanko, 2015; Petersen et al., 2020).

The rate constants describing individual transport steps are defined in Figure 1A. For modeling the pulse-chase experiment, all sterol was initially in the PM (i.e., n_1 ($t = 0$) = 1; n_2 ($t = 0$) = n_3 ($t = 0$) = n_4 ($t = 0$) = 0). We found that the model shown in Figures 1A, B accurately describes the experimentally observed time courses including the biphasic behavior of sterol transport from the PM and to the LE/LYSs in the disease cells (Figure 1D). A compartment model with only three compartments (i.e., n_1(t)-n_3(t), equivalent to cycling of sterol between PM, REs, and the membrane of LE/LYSs) could not account for the dynamics of DHE in disease fibroblasts (not shown) but was sufficient to describe DHE dynamics in control cells (Figure 1C). A reversible transport scheme, in which sterol shuttles in two independent transport branches to the REs and LE/LYSs, respectively, could also describe the DHE transport data of control cells, but failed to describe the data of disease cells (Supplementary Figure S2). Also, using the model of Figure 1A with only three compartments (equivalent to $k_4 = k_{-4} = 0$) in disease cells provided a less accurate fit in disease cells (not shown), as judged by the Akaike and Bayesian information criteria (Wagenmakers and Farrell, 2004; Daddysman and Fecko, 2013). Including an additional recycling step from REs to the PM did not improve the fit quality but resulted in higher values for the Bayesian information criterion, indicating too many fitting parameters for the available data (not shown). This does not mean, that no sterol recycles from REs to the PM but only that the existing kinetic data in human fibroblasts is insufficient to parametrize this transport step.

In summary, the biphasic sterol accumulation in the LE/LYSs of disease cells is according to our model a consequence of sterol arrival from the REs in the first late-endosomal pool (compartment 3; dashed green line in Figure 1D) followed by a slow export to the second late-endosomal pool, in which sterol accumulates after some delay (compartment 4; dotted green line in Figure 1D). We identify the first pool (n_3) with the limiting membrane of LE/LYSs and the second pool (i.e., n_4) with the ILVs. Importantly, transport from the PM to the REs and further to the endo-lysosomal membrane and back to the PM takes place with similar kinetics in control and disease cells (see Table 1 for estimated parameter values). Thus, we can allocate the affected transport step in disease cells to the slow cycling of sterol between ILVs and the limiting membrane of LE/LYSs (indicated by grey arrows in Figure 1B). Given the described function of NPC2 in accelerating sterol exchange between liposomes and in shuttling sterol to the limiting membrane of LE/LYSs (Babalola et al., 2007; Infante et al., 2008; Wang et al., 2010; Gallala et al., 2011), our model links the observed *in vitro* and proposed *in vivo* function of NPC2.

3.2 Steady state analysis of the sterol transport model allows for further comparison with experiments

Previously, we also established a continuous sterol uptake protocol from albumin, in which the sterol donor was continuously present for extended periods of time (Berzina et al., 2018). A particular advantage of the kinetic model shown above is the fact, that it paves the way for a quantitative description of DHE transport using this continuous labeling protocol as well. For that, we have to modify Eq. 1a by adding a constant inflow, v_0, and an efflux rate constant, k_5 (see Methods section 2.4 and Figure 2A). For simplicity, we assume sterol efflux taking place from the PM only. Such a pathway is suppored by numerous studies and several sterol efflux mechanisms can be envisioned from the PM, such as lipidation of ApoA1 to form high density lipoprotein (HDL) via ABCA1 and other ABC transporters, efflux to albumin, as well as release of sterol-rich vesicles from the PM, so-called ectosomes (Juhl and Wüstner, 2022). By adding a constant inflow and outflow to our model, we also can derive analytical expressions for amount of sterol in each compartment at steady state (see Supplementary Materials). By using these expressions to calculate the steady state fraction of sterol in each compartment, we find simple equations, which are independent of the inflow and efflux rates (see Supplementary Equations S2–S4). By defining $q_2 = k_4/k_{-4}$ as the equilibrium constant for sterol exchange between ILVs and limiting membrane of endo-lysosomes, one can compare the calculated sterol fraction in LE/LYSs and REs using the rate constants determined from the kinetic experiments for disease cells (Figure 2B, square; Figure 1D and Table 1) with the experimentally determined DHE intensities in LE/LYSs + REs from the continuous labeling experiment [Figure 1B at t = 0 from reference Juhl et al. (2021b)]. One finds that the model recapitulates an increased intracellular sterol fraction in NPC2-deficient cells compared to control fibroblasts (Figure 2B). However, the model underestimates the measured sterol fraction in disease cells by about 20% [i.e., $\frac{\overline{n_2}+\overline{n_3}+\overline{n_4}}{\sum_{i=1..4}\overline{n_i}}$ = 0.3961 *versus* intracellular DHE in experiments being equal to 0.495 (Juhl et al., 2021b)]. This discrepancy could be the result of three processes, which we ignore in our model; first DHE might not only be delivered to the PM in the continuous experiment but instead some DHE could be internalized together with albumin, which we found to be internalized by endocytosis in fibroblasts (Berzina et al., 2018). Second, a minor fraction of sterol delivered to cells as a complex with albumin becomes esterified by ACAT in the ER. By using lipid mass spectrometry of ^{13}C-labeled cholesterol complexed with albumin we found that this amounts to about 6% of total labeled cholesterol in control and 0.6% in NPC2-deficient fibroblasts (Berzina et al., 2018). Since, we did not consider such processes in our model, the agreement between experiment and model analysis is remarkable.

A steady state analysis can also be used to predict the behavior of an intracellular transport system for potential parameter changes (Wüstner, 2006b; Wustner, 2019). When plotting the fractional fluorescence of DHE in all three endosomal pools (i.e., the sum of LE/LYSs containing ILVs plus additionally REs; compartment 2, 3 and 4; Eq. S4) at steady state as a function of q_2, we see that cholesterol will accumulate hyperbolically for increasing q_2 (Figure 2B). Thus, our model predicts that intraluminal trapping of sterol in ILVs due to compromised transport of cholesterol from ILVs back to the limiting endo-lysosomal membrane causes the observed sterol enrichment in endo-lysosomes of NPC2 deficient cells in both the pulse-chase

10.3389/fcell.2023.1144936

TABLE 1 Parameters for DHE transport according to the compartment model shown in Figure 1 Time courses of DHE transport from the PM to REs and LE/LYSs in control and disease cells were fitted to the multi-compartment model shown in Figure 1 and Eqs 1a–d. Parameters values were optimized in parallel to all compartments by non-linear regression. The mean value, standard deviation (±) and coefficient of variation (CV) of estimated parameters is given, as provided by the SAAM software. For control cells, parameter values for rate constants k_4 and k_{-4} could not be adequately fitted, and a three-compartment model was used instead (see text for further details).

Rate constant	k_1 (min^{-1})	k_2 (min^{-1})	k_3 (min^{-1})	k_4 (min^{-1})	k_{-4} (min^{-1})
	(PM→REs)	(REs→LE/LYSs)	(LE/LYSs→PM)	(LE/LYSs→ILVs)	(ILVs→LE/LYSs)
Control cells	0.01204 ± 0.0012	0.2465 ± 0.0033	0.09351 ± 0.011	-	-
	CV = 0.0970	CV = 0.1355	CV = 0.1156		
Disease cells	0.03216 ± 0.0032	0.4331 ± 0.0049	0.1744 ± 0.0026	0.0084 ± 0.0021	0.0039 ± 0.0015
	CV = 0.0990	CV = 0.1134	CV = 0.1495	CV = 0.3961	CV = 0.2463

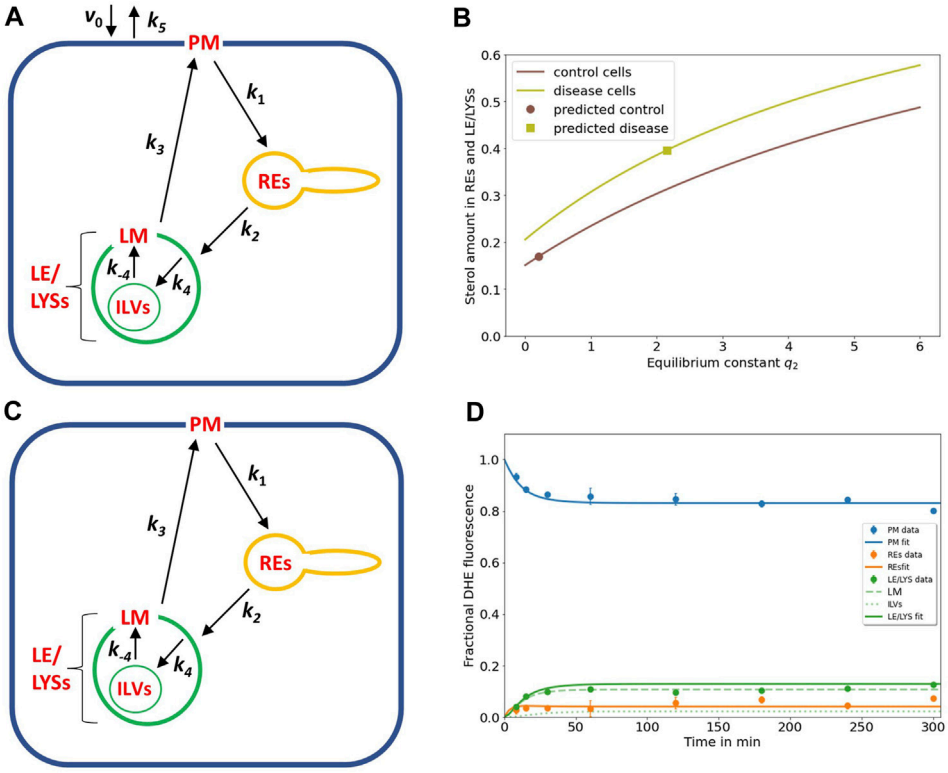

FIGURE 2
NPC2-mediated sterol transfer between ILVs and limiting membrane of endo-lysosomes determines the extent of intracellular sterol accumulation. **(A)**, extension of the kinetic model by including sterol influx with constant rate v_0 and efflux from the PM with rate constant k_5 allows for a steady state analysis (see text and Eqs S1–S4). **(B)**, the sterol fraction in REs and LE/LYSs relative to total cellular sterol was calculated according to Eq. S4 and is plotted as function of the equilibrium constant between ILVs and the endo-lysosomal membrane (i.e., $q_2 = k_4/k_{-4}$) for control cells (brown line) and NPC2-deficient cells (light green line), respectively. The calculated sterol fraction for the value of q_2 obtained by comparing the model with the experiments is indicated by a brown circle for control cells and a light green square for disease cells, respectively. **(C,D)**, the full model with sub-compartmentalized LE/LYSs was applied to the data of control cells, assuming that sterol exchange between ILVs (A, C, thin green lines) and the limiting membrane of endo-lysosomes is restored in the presence of NPC2 (A, C, thick green lines, and black arrows inside green LEL/LYSs with rate constants k_4 and k_{-4}). **(D)**, experimental data for intensity of DHE in control fibroblasts (symbols) is compared to the simulated full model with estimated parameter values for rate constants k_1 to k_3 (see Table 1) and inferred rate constants $k_4 = 0.01686$ min^{-1} and $k_{-4} = 0.0843$ min^{-1} corresponding to a ratio of $q_2 = k_4/k_{-4} = 0.2$ for the sterol fraction. For these conditions, most sterol in LE/LYSs would reside in the limiting membrane (LM, dashed green line) and much less in ILVs (dotted green line) compared to disease cells (see Figure 1D). See text for further information.

and continuous sterol uptake experiments. The same model analysis can also be used to predict an upper limit for q_2 to restore this transport defect in the presence of NPC2. For that, we ask how much the sterol equilibrium between ILVs and limiting membrane must be shifted to obtain the experimentally determined fraction of DHE in LE/LYSs of control cells. We find that one needs the ratio q_2 to be significantly smaller than one to ensure that the combined sterol fractional in LE/LYS and

REs resembles that found in control cells at steady state (Figure 2B; brown curve).

To test this conclusion, we carried out simulations of the full model with parameters determined for control cells (Table 1) and the rate constants k_4 and k_{-4} set to two and ten times the value for k_4 found in disease cells, respectively (i.e., $k_4 = 0.01686\ min^{-1}$ and $k_{-4} = 0.0843\ min^{-1}$). This corresponds to a ratio of $q_2 = 0.2$, and as shown in Figure 2D, results in good agreement between experiment and simulation. While there is much less sterol in LE/LYSs of control compared to disease cells, there is a comparable amount of sterol in the limiting membrane of LE/LYSs of both cell types (compare Figures 1D, 2D, green straight and dashed lines). These results show that the full model can describe the intracellular transport kinetics of DHE in both control, and disease cells very well.

Together, imaging-based kinetic modeling predicts that the affected step in the NPC2 disease state is the intra-endosomal sterol exchange described in our model by the rate constants k_4 and k_{-4}. Moreover, our analysis suggests that NPC2 increases sterol transport from ILVs back to the limiting late-endosomal membrane (rate constant k_{-4}) more than transport in the opposite direction (i.e., rate constant k_4). As a consequence, cholesterol and other lipids should accumulate in ILVs of NPC2-deficient fibroblasts, but not in fibroblasts from healthy subjects. This would mean, that ILVs should contain more lipid and likely become larger due to the increased lipid content in disease compared to control cells. To test this prediction, high resolution microscopy of lipid content in ILVs *versus* endo-lysosomal membrane would be needed. Since optical microscopy lacks the resolution to resolve the ultrastructure of LE/LYSs, we employed SXT for this task, as described in the next paragraph.

3.3 Soft X-ray tomography of endo-lysosomes reveals lipid enrichment in ILVs of NPC2-deficient cells

SXT is a form of X-ray microscopy gaining increasing attention as an alternative to electron microscopy (EM) for obtaining high resolution ultrastructural information of cellular architecture (McDermott et al., 2009). SXT uses the short wavelength of X-rays of 4.4 nm (corresponding to the K-edge absorption of carbon, 284 eV) to 2.3 nm (the K shell absorption edge of oxygen, 543 eV) to generate absorption contrast in the so-called water window, where carbon-rich material, such as lipid membranes absorb strongly, while water is transparent (McDermott et al., 2009; Schneider et al., 2010). SXT of cryo-frozen cells provides an isotropic resolution of about 40 nm, does not require sectioning and is of higher acquisition speed compared to EM (Schneider et al., 2010). While SXT is based on natural absorption contrast, the technique can be correlated with corresponding fluorescence images, which, however, are mostly diffraction-limited and therefore of much lower resolution (Hagen et al., 2012; Schneider et al., 2012; Duke et al., 2014). We have recently shown that extracellular vesicles, secreted from cells during cholesterol efflux, also contain the cholesterol analogue TF-Chol as well as fluorescent NPC2 (Juhl et al., 2021b). For that, 3D reconstructions of X-ray tomograms were aligned with the corresponding cryo fluorescence image of TF-Chol. Here, we use the same correlative approach and find by SXT that many intracellular vesicles in human fibroblasts contain ILVs (Figure 3A). From the corresponding fluorescence images, one finds that the same region is strongly labeled with the fluorescent cholesterol analogue, TF-Chol (Figures 3B, C). Unfortunately, due to the tight packing of vesicles in fibroblasts and the much lower resolution of fluorescence microscopy compared to SXT, we cannot correlate the LE/LYSs between both imaging modalities individually. In contrast to EM, it is more straightforward in SXT to image entire subcellular organelles in 3D. This allows for stepping through the volume of multivesicular LE/LYSs and thereby for assessing the whole population of ILVs. We find by SXT, that endo-lysosomes contain numerous ILVs in both control cells (Figures 3D–F) and disease cells (Figures 3G–I), but those ILVs are darker and larger in NPC2-deficient cells compared to control cells (compare arrows in Figures 3D, G). The appearance of dark intraluminal membranes in disease cells indicates that they contain more lipids than ILVs in control cells. This can be concluded based on the extent of X-ray absorption, which is linearly proportional to the carbon content (Schneider et al., 2010; Duke et al., 2014; Juhl et al., 2021b; Okolo et al., 2021). Non-lamellar lipid deposits are also possible, but those cannot be distinguished from small ILVs by SXT. Importantly, when treating cells with 100 nM NPC2 protein purified from bovine milk, intraluminal membrane dispositions are strongly reduced and multivesicular endo-lysosomes look similar as in control cells (compare Figures 3D–F, J–L). Together, these results show that the lack of NPC2 results in strong lipid enrichment, specifically in ILVs in human fibroblasts, and that adding back purified NPC2 protein can rescue this phenotype.

3.4 The model with sterol release only from the cell surface underestimates cellular sterol efflux

The results above show, that the multi-compartment model describes the experimental data on sterol uptake and intracellular transport well, and that its predictions are supported by SXT of LE/LYSs in control and disease cells. Our next goal is to determine, whether the model can be used to analyze cholesterol efflux from cells as well. It has been shown in several studies, that when extracellular sterol sources are removed from the medium, NPC disease cells are severely impaired in mobilizing their lysosomal sterol pool compared to control cells (Neufeld et al., 1999; Naureckiene et al., 2000; Rosenbaum et al., 2010). However, it is debated, by which pathway the excess cholesterol can be released from cells, and whether the endo-lysosomal cholesterol destined for efflux must pass through the PM (Rosenbaum et al., 2010; Vacca et al., 2019; Juhl et al., 2021b; Juhl and Wüstner, 2022). We showed recently that human fibroblasts release sterol-rich vesicles of varying sizes during efflux and observed that at least a portion of such vesicles were shed directly from the PM (Juhl et al., 2021b). Such so-called ectosomes have been observed in a variety of cell systems, and they have been associated with cholesterol efflux in several cell types, for example, in macrophages and in migrating cancer cells (Ma et al., 2015; He et al., 2018; Juhl and Wüstner, 2022). We found that the abundance of vesicles released from cells correlates with the activity of ABCA1 at the PM, which might work in tandem with NPC2 to export cholesterol from cells (Juhl et al., 2021b). But is this the only pathway for efflux of excess cholesterol from LE/LYSs? Our model predicts that DHE intensity in

10.3389/fcell.2023.1144936

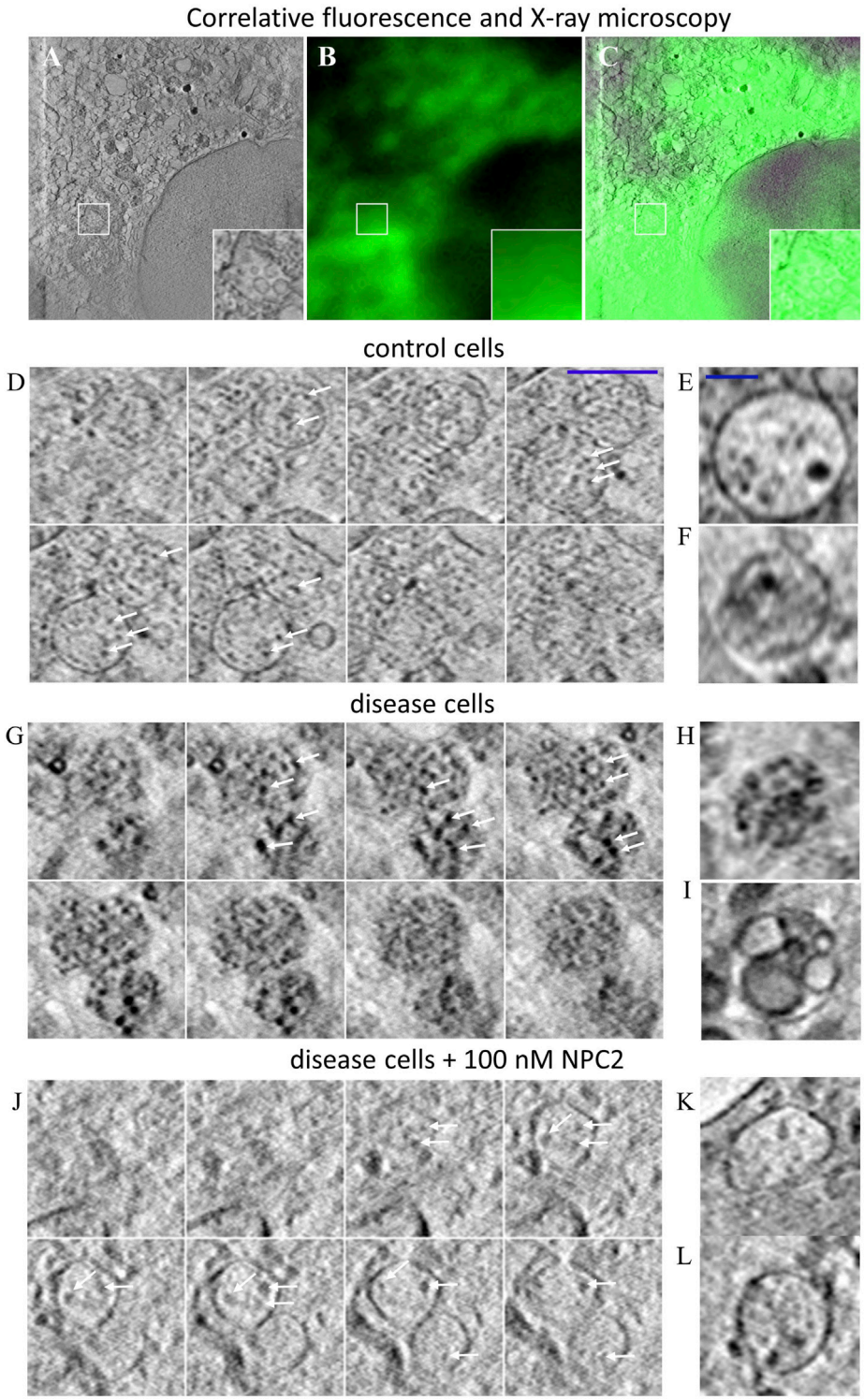

FIGURE 3
Correlative fluorescence and X-ray microscopy reveal enlarged and lipid-rich intraluminal vesicles in NPC2-deficient fibroblasts. Human fibroblasts were labeled with the cholesterol analogue TopFluor-cholesterol, cryo-frozen and imaged by soft X-ray tomography at the Synchrotron BESSY II as described in Materials and methods. **(A–C)**, correlative X-ray and fluorescence imaging of an NPC-deficient fibroblast showing the sum projection of five central image planes from a reconstructed X-ray tomogram (A, inset shows zoomed box with an endo-lysosome containing ILVs), the corresponding fluorescence image of TopFluor-cholesterol **(B)** and the overlay **(C)**. **(D–L)**, montage of X-ray reconstructions of multivesicular LE/LYSs with luminal content in control cells **(D–F)**, and NPC2-deficient cells **(G–L)**, either left untreated **(G–I)** or treated with 100 nM NPC2 for 48 h **(J–L)**. Shown are sum projections of three consecutive frames corresponding to a depth of field of 58.8 nm calculated along a 3D stack reconstructed from each X-ray tomogram. Arrows point to ILVs, which are small and almost transparent in control cells but larger and dark in disease cells due to enrichment of carbon in lipid depositions. Treatment with purified NPC2 reduces dark luminal content of endo-lysosomes, indicating removal of the lipid deposits. Small panel to the right show additional examples of multivesicular LE/LYSs of control cells **(E,F)**, untreated disease cells **(H,I)** and disease cells treated with NPC2 **(K,L)**. See main text for more information.

10.3389/fcell.2023.1144936

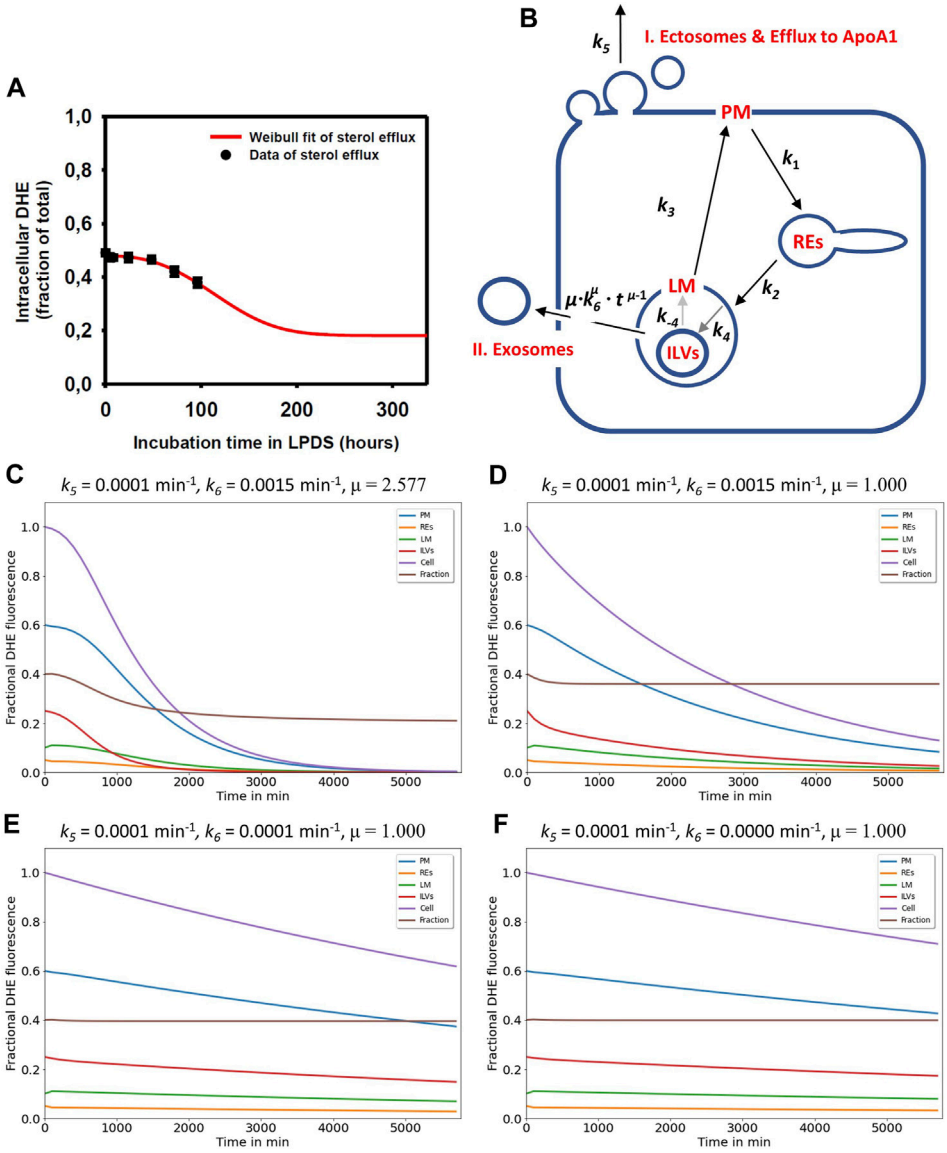

FIGURE 4
Simulation of cholesterol efflux via two pathways reconciles measured efflux kinetics in NPC2-deficient cells. **(A)**, the measured efflux kinetics of DHE from human fibroblasts lacking functional NPC2 is expressed as fractional intracellular intensity (black symbols) and reproduced from Figure 1 of (Juhl et al., 2021b) with permission. The data is fit to a Weibull survival function (red line) allowing for extrapolation of the efflux kinetics beyond the measured 96 h. **(B)**, the efflux model is based on the full compartment model and includes additionally sterol efflux from the PM via release of ectosomes and efflux to ApoA1 (I.) as well as sterol efflux directly from LE/LYSs via release of ILVs as exosomes (II.). **(C–F)**, simulation of cholesterol efflux from disease cells for different parameter combinations for sterol efflux, i.e., rate constants k_5 and k_6 and the shape parameter μ were varied, while rate constants k_1 to k_{-4} were fixed to the values determined for NPC2-deficient cells (see Table 1). Simulated time courses are shown for PM (blue lines), REs (orange lines), the limiting membrane of endo-lysosomes (green lines, 'LE/LYS'), the ILVs (red lines) and the total cell (violet lines). In addition, the entire intracellular sterol pool (i.e., sum of REs, LM and ILVs) was calculated and normalized to the total cellular pool (brown lines). This calculated intracellular sterol fraction can be directly compared to the experimentally determined fractional DHE intensity in cells (compare panel A with brown lines in panels **(C–F)**. Clearly, the efflux parameter combinations derived for disease cells and shown in panel **(C)** fit the data best. See main text for further explanations.

cells is 4.5fold higher in disease compared to control cells at the end of the loading period (see Supplementary Materials). In contrast, we found in experiments, that for both, DHE and ^{13}C-cholesterol, the sterol amount delivered to NPC2-deficient cells was only about 2.5fold that found in control cells [see Figure 6A in reference Berzina et al. (2018)]. Thus, our model underestimates the efficiency of sterol efflux, and there must be additional efflux pathways at play apart from cholesterol release from the PM.

3.5 A lag time model describes sterol efflux from cells via formation of exosomes and ectosomes

By measuring the time course of DHE in LE/LYSs of disease cells, we found previously that the decay of fractional fluorescence of DHE in endo-lysosomes accelerates over time (Juhl et al., 2021b). We showed that this measured time course of

sterol in LE/LYSs can be well described by a stochastic compartment model based on a Weibull survival function in NPC2-deficient cells (Juhl et al., 2021b). This data and the model prediction are replotted in Figure 4A. The survival function of the Weibull distribution is given by (Macheras and Iliadis, 2006):

$$S(t) = \exp\ (-(t/\tau)^{\mu}) \tag{3}$$

Here, τ is the time constant describing the characteristic time for a sterol molecule to reside ('survive') in LE/LYSs before release, and μ is a stretching exponent or shape parameter. For μ > 1 the Weibull survival function models delayed transport processes with an initially delayed but accelerating transport rate, while for μ = 1, a single-exponential decay with constant export rate constant is recovered (Macheras and Iliadis, 2006). The corresponding differential equation describing the rate of change of sterol molecules in LE/LYSs can be found by differentiating the survival function with respect to time, which gives:

$$\frac{S(t)}{dt} = -\mu \cdot \left(\frac{1}{\tau}\right)^{\mu} \cdot t^{\mu-1} \cdot \exp\left(-(t/\tau)^{\mu}\right) = -\frac{\mu}{\tau} \cdot \left(\frac{t}{\tau}\right)^{\mu-1} \cdot \exp\left(-(t/\tau)^{\mu}\right) \tag{4}$$

By weighting Eq. 3 with the initial fractional fluorescence of DHE in LE/LYSs of NPC2 deficient cells and adding an off set to account for the remaining intensity at steady state, we could estimate efflux parameters for sterol from fibroblasts. We found that this modified Weibull function described sterol efflux very well, providing a time constant for sterol efflux of τ = 135.14 h and μ = 2.577 in NPC2 deficient cells (Juhl et al., 2021b). It also allows for extrapolating sterol efflux beyond experimentally accessible time scales, as shown in Figure 4A (red curve). This model describes the observed phenomenon that lysosomal sterol export is delayed in the beginning of the efflux experiment but accelerates over time. Treating disease cells with purified NPC2 shortened and narrowed the retention time resulting in τ = 86.96 h and μ = 1.324 (Juhl et al., 2021b). The Weibull function with μ > 1 is also called a compressed exponential, and a physical motivation for using it in modeling lysosomal sterol efflux of disease cells is the heterogeneous transport dynamics of LE/LYSs to the PM before releasing their cargo by exocytosis. We showed previously that endo-lysosomes containing fluorescent NPC2 and DHE undergo a combination of diffusion and active transport in human fibroblasts, justifying the use of this model for analysis of sterol efflux (Lund et al., 2014; Berzina et al., 2018; Juhl et al., 2021b).

To account for this time-delayed and selective efflux of DHE from LE/LYSs, we included two efflux processes into the compartment model, a rate constant describing sterol release from the PM (k_5), as before, now specified as formation of ectosomes and/or efflux to ApoA1 (Figure 4B, pathway I), and a time-dependent rate coefficient $k(t) = \mu \cdot k_6{}^{\mu} \cdot t^{\mu-1}$ to account for the initially delayed sterol release from endo-lysosomes by exocytosis of ILVs as exosomes (Figure 4B, pathway II). Here, μ resembles the shape parameter of the Weibull survival function and k_6 the inverse of the time constant, τ. A numerical simulation of the ODE system described in Materials, section 2 and in Supplementary Materials for the initial sterol fractions in each compartment corresponding to the beginning of the efflux experiment is shown in Figures 4C–F. Kinetic parameters k_1 to k_{-4} were set to the values found for disease cells (see Table 1), while the rate constants k_5 and k_6 and the shape parameter μ were varied as shown on top of each panel in Figures 4C–F. The model does not take homeostatic mechanisms into account which would likely prevent total cellular cholesterol efflux, nor does it account for *de novo* sterol synthesis, which could replace the released sterol pool. It is instead simply concerned with analysis of the transient kinetics of sterol export from cells, which we determined experimentally for disease cells in our previous study (Juhl et al., 2021b). Importantly, for μ = 2.577, as previously determined in sterol efflux experiments in NPC2-deficient cells, a characteristic initial delay was found for the sterol amount in the ILVs, the lysosomal membrane and the PM (Figure 4C, red, green, and blue curve), respectively. The total cellular sterol also decayed after an initial delay phase (Figure 4C, violet curve). The sum of sterol in ILVs and endo-lysosomal membrane divided by the total cellular sterol gives the sterol fraction in endo-lysosomes, which resembles the experimentally accessible time course from our previous experiments (Figure 4C, brown curve, and (Juhl et al., 2021b)). It shows an initial delay and drops to a steady state value after ca. 200h, corresponding to 1,200 min. This is in good agreement with the efflux kinetics we determined previously for disease cells based on parameter fitting of the Weibull function to the efflux kinetics, which could be measured up to 96 h (compare Figure 4A red curve and Figure 4C, brown curve) (Juhl et al., 2021b). In contrast, this ratio - the sterol fraction in endo-lysosomes - drops exponentially initially and remains constant for longer times, if μ = 1.0 for the same remaining parameters (Figure 4D, brown curve). This is because efflux becomes exponential for both compartments, the PM and LE/LYSs, for μ = 1.0, and since $k_6 > k_5$, the decay from LE/LYSs is slightly faster than sterol efflux from the PM. As a consequence, one would find a slight exponential drop in the ratio of sterol in endo-lysosomes *versus* total cell, if lysosomal exocytosis would follow a mono-exponential kinetics. This, however, was not observed in cells (Figure 4A), showing that the time-delay in lysosomal sterol exocytosis is needed to accurately describe the experimental data. If one sets additionally the rate constant for sterol export from LE/LYSs equal to the one for sterol release from the PM (i.e., $k_6 = k_5$), the sterol fraction in LE/LYSs becomes a constant rapidly, while the amount of sterol in the PM drops slowly and in an exponential manner (Figure 4E, brown and blue curve), respectively. If we set the rate constant for sterol efflux from LE/LYSs via exocytosis of ILVs as exosomes to zero (i.e., $k_6 = 0$), only sterol efflux from the PM remains (Figure 4F). Importantly, also under those conditions, sterol drops very slowly in all intracellular compartments since they are connected to the PM, from where sterol is released as ectosomes and/or lipidation of ApoA1 (Figure 5F, with rate constant $k_5 = 0.0001\ \text{min}^{-1}$). However, the sterol fraction in endo-lysosomes stays constant and equal to the initial value at the start of the efflux experiment under these conditions (Figure 4F, brown curve). These results show that sterol efflux from the PM alone is not sufficient to explain the preferential

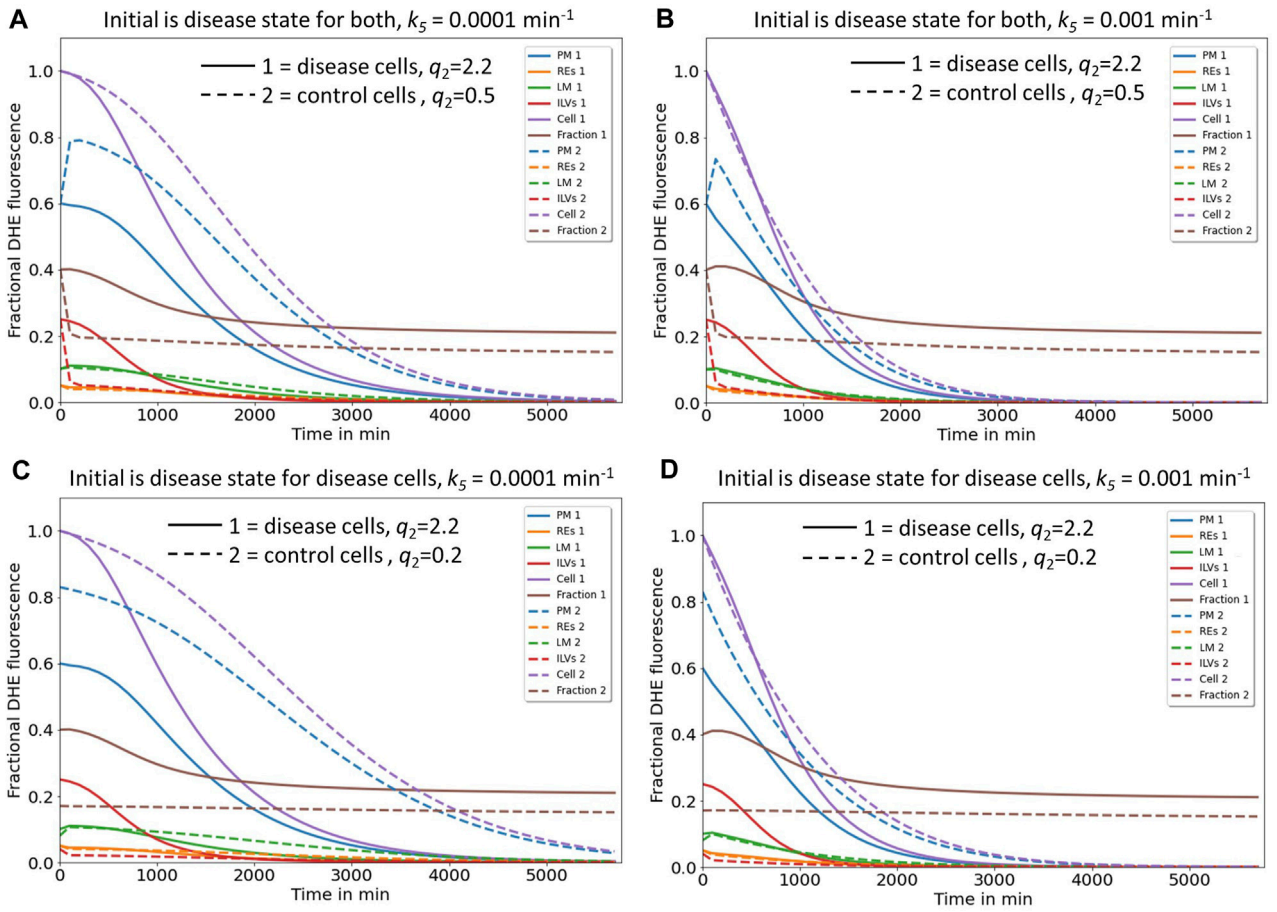

FIGURE 5
Simulation of cholesterol efflux from control and disease cells predicts reciprocal regulation of the two identified pathways by NPC2. Simulation of cholesterol efflux from disease cells (straight lines) or control cells (dashed lines), either with initial sterol amounts in each compartment as found in disease cells **(A, B)** or as found in disease and control cells, respectively **(C, D)**. Rate constants k_6 and the shape parameter μ were kept constant at k_6 = 0.0015 min^{-1} and μ = 2.57, while rate constants k_1 to k_{-4} were fixed to the values determined for NPC2-deficient cells (straight lines and Table 1) or to the values inferred for control cells (dashed lines and Table 1). In the latter case, the rate constants k_4 to k_{-4} were set to two- and either four- or tenfold the value estimated for k_4 in disease cells, to obtain either q_2 = 0.5 or 0.2 for control cells. This simulates the more efficient transport of sterol from ILVs back to the limiting membrane of LE/LYSs in the presence of NPC2 and is indicated in the panels. Rate constant k_5, which describes sterol release from the PM, was varied as described on the top of each panel. Simulated time courses are shown for PM (blue lines), REs (orange lines), the limiting membrane of endo-lysosomes (green lines, 'LE/LYS'), the ILVs (red lines) and the total cell (violet lines). Also, the entire intracellular sterol pool (i.e., sum of REs, LM and ILVs) was calculated and normalized to the total cellular pool (brown lines). One finds that total sterol drops faster in disease than in control cells, if the rate constant for sterol efflux from the PM, k_5, is low (C, straight and dashed violet lines). Also, for control and disease cells increasing k_5 ten-fold accelerates the drop in total and PM sterol, but it does not change the intracellular sterol fraction (compare C and D; brown dashed and straight lines). See main text for further explanations.

efflux of sterol from endo-lysosomes, which we observed by measuring the sterol fraction in endo-lysosomes (Figure 4A, red curve) (Juhl et al., 2021b). It needs an additional mechanism, which removes sterol *selectively* from endo-lysosomes *bypassing* the PM, as otherwise the sterol fraction in endo-lysosomes would be constant despite continuous sterol release from cells. By extending our model to include a second efflux process of cholesterol directly from endo-lysosomes (Figure 4B, pathway II), we can achieve good agreement between experimentally observed sterol efflux and model predictions. This is a central conclusion of this model analysis. We suggest that this second mechanism is the release of exosomes, i.e., lysosomal exocytosis of ILVs, which has been observed in NPC1-deficient fibroblasts and neuronal cells (Figure 4B) (Strauss et al., 2010; Demais et al., 2016; Ilnytska et al., 2021a; Guix et al., 2021). This efflux process is well-described by a compressed exponential or Weibull-type export rate. The mechanism underlying this delayed efflux is likely the heterogenous diffusion and transport of LE/LYSs towards the PM followed by lysosomal exocytosis.

3.6 Reciprocal regulation of sterol efflux via release of exosomes and ectosomes by NPC2 activity

Next, we asked, how these two efflux mechanisms, i.e., sterol release from the PM, either as ectosomes or by lipidation of ApoA1 (pathway I) and sterol efflux by lysosomal exocytosis (pathway II) could be coordinated and how NPC2 might control these processes. For that we simulated the time courses given by the differential

equation system consisting of Eqs. S6a, 1b, 1c and S6b with the rate constants determined for disease cells and for control cells, respectively (Figure 5 straight and dashed lines). Total sterol at the beginning of the efflux simulations was set to one to be able to compare control and disease cells. For rate constants k_4 and k_{-4} a two- and fourfold higher value was assumed for control cells than that found in disease cells, which is in line with our analysis of the pulse-chase and continuous uptake experiments (Figure 2). This will account for faster intraluminal sterol transfer from ILVs to the limiting endo-lysosomal membrane in the presence of NPC2. The initial amount of sterol in each compartment and the μ-parameter describing the delayed sterol efflux by release of exosomes corresponded to that found under cholesterol accumulation conditions, i.e., in disease cells. Thus, we assessed how excess cholesterol will be exported from cells if the kinetic parameters for sterol transport between LE/LYSs and PM resemble those of either disease or control cells. Simulating this scenario, we find that the combined sterol fraction in the endo-lysosomal membrane and ILVs normalized to total cellular sterol decay much slower in disease than in control cells (Figures 5A, B, straight and dashed brown curves). This is in line with the experimentally observed shortening of the sterol retention time in disease cells treated with NPC2 protein (Juhl et al., 2021b). According to our model, the sterol amount in the PM drops in a sigmoid fashion in disease cells but exceeds the initial amount transiently in control cells before eventually decreasing for longer times (Figures 5A, B, straight and dashed blue curves). Both, the transient increase of sterol in the PM and the rapid sterol decrease in the lysosomal sterol fraction in control cells are a consequence of the faster delivery of the sterol pool from ILVs to the limiting membrane of LE/LYSs in the presence of NPC2. This rapidly replenishes sterol delivered from the lysosomal membrane to the PM in these cells. The faster delivery of sterol to the PM and sterol export from LE/LYSs in control cells cannot be due to faster lysosomal exocytosis, since the parameters for this process are the same for simulations of control and disease cells (i.e., $k_6 = 0.01\ s^{-1}$ and $\mu = 2.577$). This was chosen by intention to compare the effect of intracellular sterol trafficking on efflux kinetics. In reality, the delay parameter μ could be affected by NPC2, as we observed a narrower retention time of sterol upon treating disease cells with purified NPC2 (Juhl et al., 2021b). This effect is analyzed further below.

Interestingly, in our simulations total cellular sterol release is more efficient for disease cells, as long as shedding of ectosomes from the PM is slow (Figure 5A, straight and dashed violet line). We see from that analysis, that secretion of sterol-rich ILVs due to lack of NPC2 mediated intraluminal sterol transfer in disease cells causes a more pronounced net sterol efflux than release of sterol-poor exosomes, found in control cells. Increasing the rate of sterol efflux from the PM, on the other hand, has a proportionally larger effect in control cells, where sterol delivery from ILVs to the limiting membrane of LE/LYSs is more efficient (Figure 5B, straight and dashed violet line). Still, our model predicts that boosting cholesterol efflux from the PM will also alleviate sterol export in disease cells. This prediction of our model agrees with our recent findings, that upregulation of ABCA1 together with ABCA1 causes a drop in PM sterol but only little change in intracellular cholesterol (see Fig. 8 in (Juhl et al., 2021b)). Only when adding NPC2 protein to the culture medium, intracellular cholesterol will be additionally removed, exactly as predicted by our model.

Supporting the notion of a reciprocal regulation between both efflux pathways are additional simulations, in which we compare the impact of initial conditions in each compartment (Figures 5C, D). In disease cells, the sterol fraction in LE/LYSs drops in a sigmoid fashion for high initial sterol as found in the absence of NPC2 (Figures 5C, D, straight brown line). In contrast, if we set the initial conditions to low sterol amounts and use kinetic parameters as found in control cells, no change of the sterol fraction in endo-lysosomes is found (Figures 5C, D, dashed brown line). This is the case despite overall cellular sterol efflux in control cells and for 10-fold varying release rate constants, k_5, from the PM (Figures 5C, D, dashed violet line). Thus, our model predicts that the sterol fraction in endo-lysosomes of control cells should be constant despite continuous sterol efflux from cells. We can test this prediction by measuring efflux of DHE from control fibroblasts, where we find that the fraction of DHE in LE/LYSs labeled with fluorescent dextran indeed stays constant over an efflux period of 72h, even though total cell-associated DHE decreases severalfold (Supplementary Figure S3). Thus, our model can describe sterol efflux from both, control and disease cells equally well. Additional analysis shows that adding NPC2 protein to disease cells can indeed accelerate sterol mobilization from LE/LYSs and thereby enhance sterol efflux from the cells, as we observed in experiments [Supplementary Figure S4 and Juhl et al. (2021b)].

Our results can be summarized as follows (Figure 6): in control cells, cholesterol is efficiently transported from ILVs back to the limiting membrane of LE/LYSs, therefore being available for transport to the PM and efflux from cells. Therefore, the first efflux pathway via ectosomes and lipid export to ApoA1 is contributing more to net sterol efflux (Figure 6A). In disease cells, intraluminal sterol transport in LE/LYSs is hindered and cholesterol accumulates in ILVs due to lack of NPC2. Since ILVs are the precursors for exosomes, more sterol is available for lysosomal exocytosis, i.e., pathway II, in disease cells (Figure 6B). The latter has indeed been observed in NPC1-deficient cells (Strauss et al., 2010; Demais et al., 2016; Guix et al., 2021). We conclude from this analysis, that sterol efflux by release of exosomes and by shedding from the PM are reciprocally regulated by the intraluminal sterol transfer activity of NPC2 inside endo-lysosomes.

4 Discussion

Recent structural and mechanistic studies have provided novel insight into the molecular function of NPC1 and NPC2 in cholesterol export from LE/LYSs. However, the regulation of dynamic sterol shuttling between PM and endo-lysosomes, and the efflux of excess lysosomal cholesterol from particularly NPC2-deficient cells are little understood. Precise quantitative measurements of intracellular sterol transport combined with mathematical modeling of the transport kinetics can provide new insight into these processes. Here, we have developed a mathematical model of sterol trafficking between PM and endo-lysosomes in human fibroblasts. We show that sterol trafficking to LE/LYSs via REs is in line with the available kinetic data on sterol transport in fibroblasts, thereby extending previous modeling attempts for this pathway (Lange et al., 1998). Our model shows that the overall transit time defined as sum of the reciprocal rate

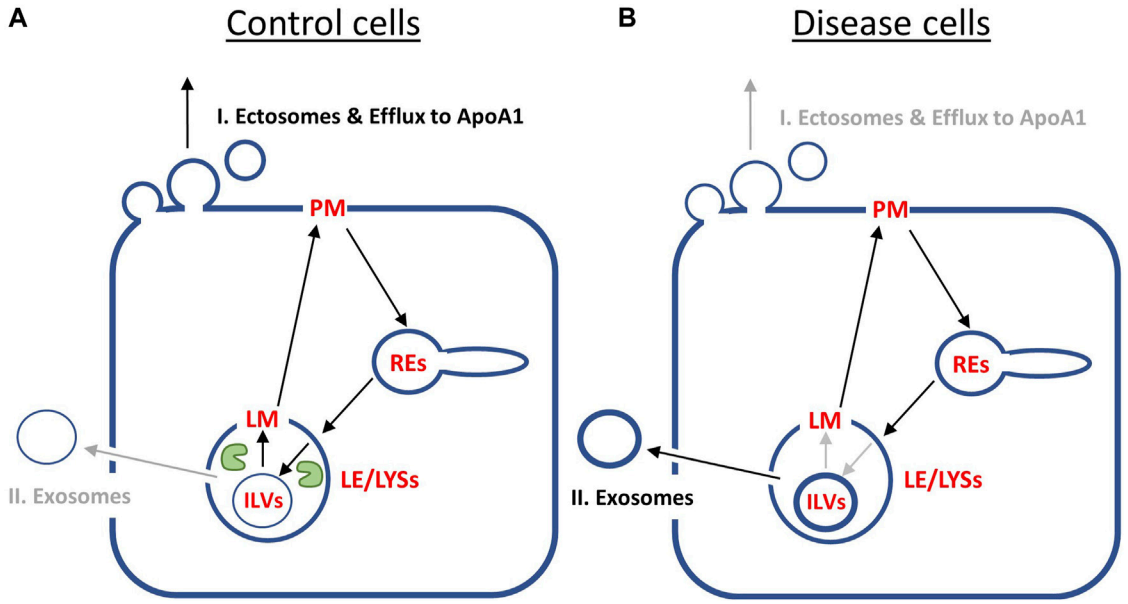

FIGURE 6
Summary of model predictions on reciprocal regulation of cholesterol efflux pathways by NPC2 activity inside endo-lysosomes. **(A)**, in control cells, NPC2 protein inside LE/LYSs (green 'pac man') mediates efficient cholesterol transfer from ILVs to the limiting membrane (LM) of endo-lysosomes. This allows for preferred shuttling of sterol back to the PM for efflux via pathway I., i.e., sterol release from the PM as ectosomes and/or by efflux to ApoA1. Therefore, the cholesterol content of ILVs is low (thin blue ring inside LE/LYSs in A), and only little sterol will efflux via pathway II, i.e., lysosomal exocytosis and release of exosomes. **(B)**, in disease fibroblasts, the lack of NPC2 results in slow and inefficient cholesterol transfer between ILVs and LM of LE/LYSs. As a consequence, cholesterol build's up in ILVs (thick blue ring inside LE/LYSs in B). This results in preferred cholesterol efflux via pathway II, i.e., secretion of exosomes, which are nothing but transformed ILVs released from cells. See text for further explanations.

constants between PM, REs and endo-lysosomes (i.e. $1/k_1+1/k_2+1/k_3$) is about 1.5 h in control cells (Krzyzanski, 2011), supporting earlier suggestions, that LE/LYSs can rapidly respond to changes in PM cholesterol (Lange et al., 1998; Castellano et al., 2017). Our results also support previous findings questioning the general view that initial sterol export from endo-lysosomes is defective in NPC-disease cells (Cruz et al., 2000; Lange et al., 2000). In fact, kinetic modeling suggests that sterol cycling between the limiting membrane of LE/LYSs, and the PM is at least as fast in NPC2-deficient cells as in control fibroblasts (Table 1 and above). In fact, the transit time for sterol between PM, REs and limiting membrane of LE/LYSs is about 40 min in disease cells, i.e., faster than in control cells, when using the respective mean values of the estimated rate constants, k_1, k_2 and k_3. However, we found that sterol gets trapped inside LE/LYSs leading to its removal from the sterol circuit between PM, REs and limiting membrane of LE/LYSs and instead to its build up in ILVs inside endo-lysosomes in cells lacking functional NPC2. This results in a second slow phase of sterol accumulation in LE/LYSs of NPC2-deficient cells, not observed in control cells. Using correlative SXT and fluorescence microscopy we were able to confirm enlargement of ILVs with increased lipid content in fibroblasts lacking functional NPC2, thereby supporting our model predictions.

Based on our model and previous findings (Juhl et al., 2021b), we postulate that efflux of excess endo-lysosomal cholesterol from fibroblasts can take place via two pathways, I) efflux from the PM, at least partly involving ectosome release and II) secretion of exosomes in a form of lysosomal exocytosis. We model the latter pathway via a Weibull-type differential equation. This function allows us to account for the delayed decrease in the intracellular sterol fraction in disease cells upon removal of sterol sources from the culture medium (Juhl et al., 2021b). Delays in cholesterol efflux have also been included in a previous study in macrophages, but the authors did this by postulating additional transit compartments (Gaus et al., 2001). This could also be done in our system. In fact, reasonable fits were also found for modeling lysosomal sterol export using an Erlang-type distribution in the efflux experiments (not shown). However, this requires postulating additional compartments, for which no experimental evidence is currently available. A limitation of our model is that kinetics of sterol transport through the fourth compartment, the ILVs is parametrized indirectly, i.e., without direct access to a time course of DHE transport to and from ILVs. This allows us to explain the observed biphasic increase of DHE fluorescence in LE/LYSs in the pulse-chase kinetics (Figure 1) and enables us to model sterol efflux from cells via two alternative pathways (Figures 4, 5). An alternative kinetic description allowing us to describe this biphasic sterol transport to endo-lysosomes can also be based on a Weibull-type delay model. This provides also very good fits to the pulse-chase kinetics of DHE without invoking a fourth compartment (Supplementary Figure S5). Such a model could be motivated by heterogeneous export from LE/LYSs due to trapping of sterol molecules at long times, for example, due to incomplete mixing in these compartments. In such a scenario, transport from LE/LYSs back to the PM would follow a stretched exponential decay characterized by $\mu<1$, which accounts for the trapping-induced memory in the system (Sopasakis et al., 2018). However, stretched exponential export kinetics of DHE from LE/

LYSs is not in line with our efflux experiments, in which compressed exponential kinetics (i.e., μ>1) for sterol export from endo-lysosomes was found. Mechanistically, stretched exponential kinetics corresponds to decreasing rate coefficients, i.e., slowed kinetics over time, while compressed exponential kinetics corresponds to increasing rate coefficients, i.e., accelerated kinetics over time (Wüstner et al., 2012). We conclude that incomplete mixing of DHE with an immobile sterol pool inside LE/LYSs cannot account for the observed kinetics of sterol efflux from cells.

Our modeling results suggest that both efflux pathways (i.e., sterol release from the PM via shedding of ectosomes and/or lipidation of ApoA1 *versus* lysosomal exocytosis of ILVs as exosomes) could be reciprocally regulated by the sterol transfer activity of NPC2 inside LE/LYSs: in cells lacking NPC2, the diminished transfer capacity between ILVs and the limiting membrane causes cholesterol build up in ILVs, which the affected cells clear via preferred sterol efflux by exosome secretion. In contrast, in control cells, cholesterol transfer from ILVs to the membrane of LE/LYSs is catalyzed by NPC2 resulting in efficient sterol transfer to the PM, such that the first pathway of sterol efflux should be used preferentially (Figure 6). These predictions are supported by experimental findings in NPC1 deficient neurons and glia cells, where not only more and larger ILVs were found but also more exosomes were secreted than in control cells (Strauss et al., 2010; Ilnytska et al., 2021b; Guix et al., 2021). Supplementation of NPC1-deficient fibroblasts with phosphatidylglycerol, the precursor of LBPA and other lipid species in ILVs, caused an increased release of cholesterol-rich exosomes and a downregulation of ABCA1 (Ilnytska et al., 2021a). The latter is expected if reciprocal regulation of sterol efflux from the PM via an ectosome/ABCA1 pathway and lysosomal exocytosis of exosomes is at play in cellular cholesterol efflux. LBPA, which is formed from supplemented PG, is abundant in LE/LYSs, where it can contribute up to 15–20 mol% of total phospholipids. It is likely, that LBPA location and abundance inside LE/LYSs plays a key role in this reciprocal regulation. LBPA is not only a binding partner for NPC2, enhancing interbilayer sterol transfer by NPC2 but also an activator of acid sphingomyelinase, which converts sphingomyelin into ceramide (Oninla et al., 2014). Ceramide, on the other hand, is a lipid with high negative spontaneous curvature due to its low head-group to acyl chain ratio. It is directly involved in intraluminal budding of vesicles and thereby formation of ILVs inside endo-lysosomes (Trajkovic et al., 2008). Interestingly, production of ceramide from degradation of sphingomyelin by acid sphingomyelinase increases NPC2 mediated sterol transfer between liposomes severalfold (Abdul-Hammed et al., 2010; Oninla et al., 2014). Incubating NPC1-deficient fibroblasts with purified acid sphingomyelinase ameliorates cholesterol clearance and trafficking capacity in these cells (Devlin et al., 2010).

Based on these findings it is reasonable to speculate that the gradient of these lipids, LBPA and ceramide, inside LE/LYSs could also facilitate directional sterol transfer by NPC2 between ILVs and the limiting membrane of endo-lysosomes. This, in turn, would contribute to the reciprocal regulation of the two sterol efflux pathways. Future experiments should test the model proposed here, for example, by studying intracellular trafficking and lysosomal export of cholesterol analogues in disease fibroblasts treated with PG, LBPA or acid sphingomyelinase. Similarly, sterol transport kinetics could be analyzed with our model in cells treated with mutated NPC2, in which the interaction with LBPA and with sterol transporters such as NPC1 or LAMP2 has been removed (Deffieu and Pfeffer, 2011; Li and Pfeffer, 2016; McCauliff et al., 2019). Finally, it would be very interesting to explore the link between NPC2 and lysosomal exocytosis further, as this process is known to be regulated by calcium-mediated signaling via the endo-lysosomal ion channel mucolipin-1 as well as the transcription factor TFEB, a master regulator of lysosome biogenesis (Medina et al., 2011; Medina et al., 2015). These key regulatory mechanisms could also be important drug targets to treat NPC disease by specifically upregulating the two cholesterol efflux pathways described here. In conclusion, our study shows that quantitative modeling of intracellular sterol transport and efflux combined with high-resolution multimodal imaging plays an important role in elucidating mechanisms of lipid transfer and in testing hypotheses of cellular lipid homeostasis.

Data availability statement

The raw data supporting the conclusion of this article will be made available by the authors, without undue reservation.

Ethics statement

Ethical approval was not required for the studies on humans in accordance with the local legislation and institutional requirements because only commercially available established cell lines were used.

Author contributions

DW designed the study, developed the mathematical model, fit it to the data, analyzed experimental data and wrote the first draft of the manuscript. AD prepared and labeled cells and carried out SXT measurements with help of SW, JM, and GS. JE together with AD and DW analyzed the X-ray image data. All authors contributed to the article and approved the submitted version.

Funding

Financial support from the Lundbeck foundation (grant nr. R366-2021-226), the Villum foundation (grant nr. 35865) as well as from the Danish Research Council (grant id. 10.46540/2034-00136B) to DW is acknowledged.

Acknowledgments

We thank S. Kozakijevic for technical assistance and the HZB for the allocation of synchrotron radiation beamtime at the undulator beamline U41-TXM at the BESSY II electron storage ring, Berlin, Germany.

Conflict of interest

The authors declare that the research was conducted in the absence of any commercial or financial relationships that could be construed as a potential conflict of interest.

Publisher's note

Supplementary material

The Supplementary Material for this article can be found online at: https://www.frontiersin.org/articles/10.3389/fcell.2023.1144936/full#supplementary-material

SUPPLEMENTARY FIGURE S1
Sketch of the experimental set up to measure sterol transport kinetics. Fluorescence of DHE is measured in the entire cell at each time point, t, upon thresholding each image, giving F_{cell} as function of time. Based on a binary masks generated from the images of Rh-dextran and Alexa647-transferrin (Alexa647-Tf), fluorescence of DHE is measured in LE/LYSs ($F_{LE/LYSs}$) and REs (F_{REs}), respectively. By dividing this compartmental fluorescence by the total cellular fluorescence of DHE, the fractional sterol fluorescence in each compartment is obtained. The fraction of DHE in the plasma membrane (PM) is simply the difference between one and sum of the fractional fluorescence of DHE in LE/LYSs and REs. The upper panel is reproduced from Berzina et al. (2018) with permission.

SUPPLEMENTARY FIGURE S2
Parallel and sequential models for the pulse-chase kinetic data of DHE transport. In the parallel model shown in **(A)**, DHE traffics bi-directionally in two branches originating at the plasma membrane (PM); 1) to late endosomes and lysosomes (LE/LYSs; left branch in A) or to the recycling endosomes (REs; right branch in A). In the sequential model shown in **(B)**, DHE traffics sequentially from the PM to the REs and from there to the LE/LYSs. Both models were solved numerically in SAAM software and fitted to the experimental time courses, for control cells **(C)** and for NPC2 disease cells **(D)**. The symbols show the experimental data of the DHE fraction in the PM (black circles, control cells; black triangles, disease cells), in the REs (green circles, control cells; green triangles, disease cells) and in the LE/LYSs (red circles, control cells; red triangles, disease cells). Black and brown straight lines show the fit of the parallel and sequential model, respectively, to the DHE data in the PM. Green and spinach green straight lines show the fit of the parallel and sequential model, respectively, to the DHE data in the REs. Red and orange straight lines show the fit of the parallel and sequential model, respectively, to the DHE data in the LE/LYSs. Dotted lines in D indicate a fit with the parallel model but with rate constants for the second branch between PM and REs constraint to the values found in control cells (compare green line in C). This constraint did not affect the fit of the parallel model to the time course of DHE transport from the PM to the LE/LYSs, showing the independence of both branches in this model. Overall, the fit quality of both models, as judged by the Chi-square value and Akaike criterion, was much worse compared to that for the model shown in the main text.

SUPPLEMENTARY FIGURE S3
Efflux kinetics of DHE from control cells confirm model predictions. Fibroblasts from healthy donors were labeled with DHE loaded onto albumin for 24 h in medium containing LPDS in the presence of Rh-dextran to label LE/LYSs. Cells were washed and incubated in medium with LPDS but without sterol source for additional 4, 8, 24, 48 and 72 h before imaging in buffer medium. **(A)**, representative images of DHE (upper panels) and corresponding image of Rh-dextran (middle panel) and color overlay of both markers with DHE in green and Rh-dextran in red (lower panel) for selected time points. DHE images in the upper row are equally scaled, showing that the sterol probe is efficiently efflux from cells (calibration bar with 0 to 300 intensity units in a FIRE look-up table is shown to the right). **(B)**, the fraction of DHE in LE/LYSs expressed as normalized to total cellular DHE intensity was determined using an ImageJ plugin described in Berzina et al. (2018), and it is plotted as function of time (n=8-15 cells from two independent experiments). The fractional DHE intensity in LE/LYSs is close to 0.15 and remains constant throughout the efflux experiment, exactly as predicted by the model (compare brown dashed line in Figures 5C, D). See text for further explanations. Bar, 20 µm.

SUPPLEMENTARY FIGURE S4
Simulation of rescue experiment of cholesterol efflux in NPC2-deficient cells. **(A)**, the rescue experiment carried out in our previous study consists of treating disease cells loaded with DHE for 48 h with purified NPC2 protein (100 nM for 48 h in LPDS, see Materials and methods) (Juhl et al., 2021b) with permission. The fractional DHE fluorescence in LE/LYSs was fit to a Weibull survival function giving a delay parameter, µ=1.324. **(B–E)**, numerical simulation of sterol efflux for disease cells with experimentally determined exponent for untreated cells (µ=2.577, straight lines) or treated cells (µ=1.324, dashed lines). Simulations were carried out with different parameter combinations for sterol efflux, i.e., varying rate constants k_5 and k_6 and either rate constants k_1 to k_{-4} as determined for NPC2-deficient cells (B and C) or as inferred for control cells (D and E, see Table 1). Simulated time courses are shown for PM (blue lines), REs (orange lines), the limiting membrane of endo-lysosomes (green lines, 'LE/LYS'), the ILVs (red lines) and the total cell (violet lines). In addition, the entire intracellular sterol pool (i.e., sum of REs, LM and ILVs) was calculated and normalized to the total cellular pool (brown lines). This calculated intracellular sterol fraction can be directly compared to the experimentally determined fractional DHE intensity in cells. Only when intracellular parameters are those of control cells, a significant drop of this sterol fraction is found (compare straight and dashed brown lines in B to E). Increasing additionally the rate constant for sterol release from the PM (i.e., k_5), emulating enhanced activity of ABCA1/ApoA1, additionally prevents transient sterol accumulation in the PM of those cells (blue dashed lines in D and E). See main text for further explanations.

SUPPLEMENTARY FIGURE S5
Stretched exponential model for the pulse-chase kinetic data of DHE transport. This model is an extension of the simple three-compartment. It assumes that sterol transport from the LE/LYSs back to the PM follows a negative power law behavior. This model fits the time course of DHE transport in control and disease cells well but leads to stretched exponential sterol transport from endo-lysosomes back to the PM (see Supplementary Table S1 for parameter values). A stretched exponential decay cannot reconcile the kinetics of sterol efflux from cells, which follows a compressed exponential, or positive power law. See main text and Supplementary Material for further explanations.

References

Abdul-Hammed, M., Breiden, B., Adebayo, M. A., Babalola, J. O., Schwarzmann, G., and Sandhoff, K. (2010). Role of endosomal membrane lipids and NPC2 in cholesterol transfer and membrane fusion. *J. Lipid Res.* 51, 1747–1760. doi:10.1194/jlr.M003822

Agulleiro, J. I., and Fernandez, J. J. (2015). Tomo3D 2.0--exploitation of advanced vector extensions (AVX) for 3D reconstruction. *J. Struct. Biol.* 189, 147–152. doi:10.1016/j.jsb.2014.11.009

Appelqvist, H., Nilsson, C., Garner, B., Brown, A. J., Kagedal, K., and Ollinger, K. (2011). Attenuation of the lysosomal death pathway by lysosomal cholesterol accumulation. *Am. J. Pathol.* 178, 629–639. doi:10.1016/j.ajpath.2010.10.030

Appelqvist, H., Waster, P., Kagedal, K., and Ollinger, K. (2013). The lysosome: from waste bag to potential therapeutic target. *J. Mol. Cell Biol.* 5, 214–226. doi:10.1093/jmcb/mjt022

Babalola, J. O., Wendeler, M., Breiden, B., Arenz, C., Schwarzmann, G., Locatelli-Hoops, S., et al. (2007). Development of an assay for the intermembrane transfer of cholesterol by Niemann-Pick C2 protein. *Biol. Chem.* 388, 617–626. doi:10.1515/BC.2007.063

Barrett, P. H., Bell, B. M., Cobelli, C., Golde, H., Schumitzky, A., Vicini, P., et al. (1998). SAAM II: simulation, analysis, and modeling software for tracer and pharmacokinetic studies. *Metabolism* 47, 484–492. doi:10.1016/s0026-0495(98)90064-6

Berzina, Z., Solanko, L. M., Mehadi, A. S., Jensen, M. L. V., Lund, F. W., Modzel, M., et al. (2018). Niemann-Pick C2 protein regulates sterol transport between plasma membrane and late endosomes in human fibroblasts. *Chem. Phys. Lipids* 213, 48–61. doi:10.1016/j.chemphyslip.2018.03.006

Carette, J. E., Raaben, M., Wong, A. C., Herbert, A. S., Obernosterer, G., Mulherkar, N., et al. (2011). Ebola virus entry requires the cholesterol transporter Niemann-Pick C1. *Nature* 477, 340–343. doi:10.1038/nature10348

Castellano, B. M., Thelen, A. M., Moldavski, O., Feltes, M., Van Der Welle, R. E., Mydock-Mcgrane, L., et al. (2017). Lysosomal cholesterol activates mTORC1 via an SLC38A9-Niemann-Pick C1 signaling complex. *Science* 355, 1306–1311. doi:10.1126/science.aag1417

Cheruku, S. R., Xu, Z., Dutia, R., Lobel, P., and Storch, J. (2006). Mechanism of cholesterol transfer from the Niemann-Pick type C2 protein to model membranes supports a role in lysosomal cholesterol transport. *J. Biol. Chem.* 281, 31594–31604. doi:10.1074/jbc.M602765200

Chevallier, J., Chamoun, Z., Jiang, G., Prestwich, G., Sakai, N., Matile, S., et al. (2008). Lysobisphosphatidic acid controls endosomal cholesterol levels. *J. Biol. Chem.* 283, 27871–27880. doi:10.1074/jbc.M801463200

Cox, B. E., Griffin, E. E., Ullery, J. C., and Jerome, W. G. (2007). Effects of cellular cholesterol loading on macrophage foam cell lysosome acidification. *J. Lipid Res.* 48, 1012–1021. doi:10.1194/jlr.M600390-JLR200

Cruz, J. C., Sugii, S., Yu, C., and Chang, T. Y. (2000). Role of Niemann-Pick type C1 protein in intracellular trafficking of low density lipoprotein-derived cholesterol. *J. Biol. Chem.* 275, 4013–4021. doi:10.1074/jbc.275.6.4013

Daddysman, M. K., and Fecko, C. J. (2013). Revisiting point FRAP to quantitatively characterize anomalous diffusion in live cells. *J. Phys. Chem.* 117, 1241–1251. doi:10.1021/jp310348s

Deffieu, M. S., and Pfeffer, S. R. (2011). Niemann-Pick type C 1 function requires lumenal domain residues that mediate cholesterol-dependent NPC2 binding. *Proc. Natl. Acad. Sci. U. S. A.* 108, 18932–18936. doi:10.1073/pnas.1110439108

Demais, V., Barthelemy, A., Perraut, M., Ungerer, N., Keime, C., Reibel, S., et al. (2016). Reversal of pathologic lipid accumulation in NPC1-deficient neurons by drug-promoted release of LAMP1-coated lamellar inclusions. *J. Neurosci.* 36, 8012–8025. doi:10.1523/JNEUROSCI.0900-16.2016

Devlin, C., Pipalia, N. H., Liao, X., Schuchman, E. H., Maxfield, F. R., and Tabas, I. (2010). Improvement in lipid and protein trafficking in Niemann-Pick C1 cells by correction of a secondary enzyme defect. *Traffic* 11, 601–615. doi:10.1111/j.1600-0854.2010.01046.x

Duke, E. M., Razi, M., Weston, A., Guttmann, P., Werner, S., Henzler, K., et al. (2014). Imaging endosomes and autophagosomes in whole mammalian cells using correlative cryo-fluorescence and cryo-soft X-ray microscopy (cryo-CLXM). *Ultramicroscopy* 143, 77–87. doi:10.1016/j.ultramic.2013.10.006

Estronca, L. M., Moreno, M. J., and Vaz, W. L. (2007). Kinetics and thermodynamics of the association of dehydroergosterol with lipid bilayer membranes. *Biophys. J.* 93, 4244–4253. doi:10.1529/biophysj.107.112847

Fraldi, A., Annunziata, F., Lombardi, A., Kaiser, H. J., Medina, D. L., Spampanato, C., et al. (2010). Lysosomal fusion and SNARE function are impaired by cholesterol accumulation in lysosomal storage disorders. *EMBO J.* 29, 3607–3620. doi:10.1038/emboj.2010.237

Gallala, H. D., Breiden, B., and Sandhoff, K. (2011). Regulation of the NPC2 protein-mediated cholesterol trafficking by membrane lipids. *J. Neurochem.* 116, 702–707. doi:10.1111/j.1471-4159.2010.07014.x

Garvik, O., Benediktson, P., Simonsen, A. C., Ipsen, J. H., and Wüstner, D. (2009). The fluorescent cholesterol analog dehydroergosterol induces liquid-ordered domains in model membranes. *Chem. Phys. Lipids* 159, 114–118. doi:10.1016/j.chemphyslip.2009.03.002

Gaus, K., Gooding, J. J., Dean, R. T., Kritharides, L., and Jessup, W. (2001). A kinetic model to evaluate cholesterol efflux from THP-1 macrophages to apolipoprotein A-1. *Biochemistry* 40, 9363–9373. doi:10.1021/bi010323n

Goldman, S. D., and Krise, J. P. (2010). Niemann-Pick C1 functions independently of Niemann-Pick C2 in the initial stage of retrograde transport of membrane-impermeable lysosomal cargo. *J. Biol. Chem.* 285, 4983–4994. doi:10.1074/jbc.M109.037622

Goldstein, J. L., and Brown, M. S. (2009). The LDL receptor. *Arterioscler. Thromb. Vasc. Biol.* 29, 431–438. doi:10.1161/ATVBAHA.108.179564

Goldstein, J. L., Debose-Boyd, R. A., and Brown, M. S. (2006). Protein sensors for membrane sterols. *Cell* 124, 35–46. doi:10.1016/j.cell.2005.12.022

Guix, F. X., Capitan, A. M., Casadome-Perales, A., Palomares-Perez, I., Lopez Del Castillo, I., Miguel, V., et al. (2021). Increased exosome secretion in neurons aging *in vitro* by NPC1-mediated endosomal cholesterol buildup. *Life Sci. Alliance* 4, e202101055. doi:10.26508/lsa.202101055

Hagen, C., Guttmann, P., Klupp, B., Werner, S., Rehbein, S., Mettenleiter, T. C., et al. (2012). Correlative VIS-fluorescence and soft X-ray cryo-microscopy/tomography of adherent cells. *J. Struct. Biol.* 177, 193–201. doi:10.1016/j.jsb.2011.12.012

Hao, M., Lin, S. X., Karylowski, O. J., Wüstner, D., Mcgraw, T. E., and Maxfield, F. R. (2002). Vesicular and non-vesicular sterol transport in living cells. The endocytic recycling compartment is a major sterol storage organelle. *J. Biol. Chem.* 277, 609–617. doi:10.1074/jbc.M108861200

Haynes, M. P., Phillips, M. C., and Rothblat, G. H. (2000). Efflux of cholesterol from different cellular pools. *Biochemistry* 39, 4508–4517. doi:10.1021/bi992125q

He, C., Hu, X., Weston, T. A., Jung, R. S., Sandhu, J., Huang, S., et al. (2018). Macrophages release plasma membrane-derived particles rich in accessible cholesterol. *Proc. Natl. Acad. Sci. U. S. A.* 115, E8499–E8508. doi:10.1073/pnas.1810724115

Heymann, J. B., and Belnap, D. M. (2007). Bsoft: image processing and molecular modeling for electron microscopy. *J. Struct. Biol.* 157, 3–18. doi:10.1016/j.jsb.2006.06.006

Huotari, J., and Helenius, A. (2011). Endosome maturation. *EMBO J.* 30, 3481–3500. doi:10.1038/emboj.2011.286

Ilnytska, O., Jeziorek, M., Lai, K., Altan-Bonnet, N., Dobrowolski, R., and Storch, J. (2021a). Lysobisphosphatidic acid (LBPA) enrichment promotes cholesterol egress via exosomes in Niemann Pick type C1 deficient cells. *Biochimica biophysica acta. Mol. Cell Biol. lipids* 1866, 158916. doi:10.1016/j.bbalip.2021.158916

Ilnytska, O., Lai, K., Gorshkov, K., Schultz, M. L., Tran, B. N., Jeziorek, M., et al. (2021b). Enrichment of NPC1-deficient cells with the lipid LBPA stimulates autophagy, improves lysosomal function, and reduces cholesterol storage. *J. Biol. Chem.* 297, 100813. doi:10.1016/j.jbc.2021.100813

Infante, R. E., and Radhakrishnan, A. (2017). Continuous transport of a small fraction of plasma membrane cholesterol to endoplasmic reticulum regulates total cellular cholesterol. *Elife* 6, e25466. doi:10.7554/eLife.25466

Infante, R. E., Wang, M. L., Radhakrishnan, A., Kwon, H. J., Brown, M. S., and Goldstein, J. L. (2008). NPC2 facilitates bidirectional transfer of cholesterol between NPC1 and lipid bilayers, a step in cholesterol egress from lysosomes. *Proc. Natl. Acad. Sci. U. S. A.* 105, 15287–15292. doi:10.1073/pnas.0807328105

Jacquez, J. A., and Simon, C. P. (2002). Qualitative theory of compartmental systems with lags. *Math. Biosci.* 180, 329–362. doi:10.1016/s0025-5564(02)00131-1

Juhl, A. D., Heegaard, C. W., Werner, S., Schneider, G., Krishnan, K., Covey, D. F., et al. (2021a). Quantitative imaging of membrane contact sites for sterol transfer between endo-lysosomes and mitochondria in living cells. *Sci. Rep.* 11, 8927. doi:10.1038/s41598-021-87876-7

Juhl, A. D., Lund, F. W., Jensen, M. L. V., Szomek, M., Heegaard, C. W., Guttmann, P., et al. (2021b). Niemann Pick C2 protein enables cholesterol transfer from endo-lysosomes to the plasma membrane for efflux by shedding of extracellular vesicles. *Chem. Phys. Lipids* 235, 105047. doi:10.1016/j.chemphyslip.2020.105047

Juhl, A. D., and Wüstner, D. (2022). Pathways and mechanisms of cellular cholesterol efflux-insight from imaging. *Front. Cell Dev. Biol.* 10, 834408. doi:10.3389/fcell.2022.834408

Krzyzanski, W. (2011). Interpretation of transit compartments pharmacodynamic models as lifespan based indirect response models. *J. Pharmacokinet. Pharmacodyn.* 38, 179–204. doi:10.1007/s10928-010-9183-z

Lange, Y., Steck, T. L., Ye, J., Lanier, M. H., Molugu, V., and Ory, D. (2009). Regulation of fibroblast mitochondrial 27-hydroxycholesterol production by active plasma membrane cholesterol. *J. Lipid Res.* 50, 1881–1888. doi:10.1194/jlr.M900116-JLR200

Lange, Y., Ye, J., and Chin, J. (1997). The fate of cholesterol exiting lysosomes. *J. Biol. Chem.* 272, 17018–17022. doi:10.1074/jbc.272.27.17018

Lange, Y., Ye, J., Rigney, M., and Steck, T. (2000). Cholesterol movement in Niemann-Pick type C cells and in cells treated with amphiphiles. *J. Biol. Chem.* 275, 17468–17475. doi:10.1074/jbc.M000875200

Lange, Y., Ye, J., Rigney, M., and Steck, T. L. (2002). Dynamics of lysosomal cholesterol in Niemann-Pick type C and normal human fibroblasts. *J. Lipid Res.* 43, 198–204. doi:10.1016/s0022-2275(20)30161-9

Lange, Y., Ye, J., and Steck, T. L. (1998). Circulation of cholesterol between lysosomes and the plasma membrane. *J. Biol. Chem.* 273, 18915–18922. doi:10.1074/jbc.273.30.18915

Li, J., and Pfeffer, S. R. (2016). Lysosomal membrane glycoproteins bind cholesterol and contribute to lysosomal cholesterol export. *Elife* 5, e21635. doi:10.7554/eLife.21635

Li, X., Saha, P., Li, J., Blobel, G., and Pfeffer, S. R. (2016). Clues to the mechanism of cholesterol transfer from the structure of NPC1 middle lumenal domain bound to NPC2. *Proc. Natl. Acad. Sci. U. S. A.* 113, 10079–10084. doi:10.1073/pnas.1611956113

Lu, A. (2022). Endolysosomal cholesterol export: more than just NPC1. *Bioessays* 44, e2200111. doi:10.1002/bies.202200111

Lund, F. W., Jensen, M. L. V., Christensen, T., Nielsen, G. K., Heegaard, C. W., and Wüstner, D. (2014). SpatTrack: an imaging toolbox for analysis of vesicle motility and distribution in living cells. *Traffic* 15, 1406–1429. doi:10.1111/tra.12228

Luo, J., Yang, H., and Song, B.-L. (2020). Mechanisms and regulation of cholesterol homeostasis. *Nat. Rev. Mol. Cell Biol.* 21, 225–245. doi:10.1038/s41580-019-0190-7

Ma, L., Li, Y., Peng, J., Wu, D., Zhao, X., Cui, Y., et al. (2015). Discovery of the migrasome, an organelle mediating release of cytoplasmic contents during cell migration. *Cell Res.* 25, 24–38. doi:10.1038/cr.2014.135

P. Macheras and A. Iliadis (Editors) (2006). *Modeling in biopharmaceutics, pharmacokinetics, and pharmacodynamics* (New Yrok: Springer).

Maxfield, F. R., and Mcgraw, T. E. (2004). Endocytic recycling. *Nat. Rev. Mol. Cell Biol.* 5, 121–132. doi:10.1038/nrm1315

Mccauliff, L. A., Langan, A., Li, R., Ilnytska, O., Bose, D., Waghalter, M., et al. (2019). Intracellular cholesterol trafficking is dependent upon NPC2 interaction with lysobisphosphatidic acid. *Elife* 8, e50832. doi:10.7554/eLife.50832

Mccauliff, L. A., Xu, Z., and Storch, J. (2011). Sterol transfer between cyclodextrin and membranes: similar but not identical mechanism to NPC2-mediated cholesterol transfer. *Biochemistry* 50, 7341–7349. doi:10.1021/bi200574f

Mcdermott, G., Le Gros, M. A., Knoechel, C. G., Uchida, M., and Larabell, C. A. (2009). Soft X-ray tomography and cryogenic light microscopy: the cool combination in cellular imaging. *Trends Cell Biol.* 19, 587–595. doi:10.1016/j.tcb.2009.08.005

Medina, D. L., Di Paola, S., Peluso, I., Armani, A., De Stefani, D., Venditti, R., et al. (2015). Lysosomal calcium signalling regulates autophagy through calcineurin and TFEB. *Nat. Cell Biol.* 17, 288–299. doi:10.1038/ncb3114

Medina, D. L., Fraldi, A., Bouche, V., Annunziata, F., Mansueto, G., Spampanato, C., et al. (2011). Transcriptional activation of lysosomal exocytosis promotes cellular clearance. *Dev. Cell* 21, 421–430. doi:10.1016/j.devcel.2011.07.016

Meurer, A., Smith, C. P., Paprocki, M., Čertík, O., Kirpichev, S. B., Rocklin, M., et al. (2017). SymPy: symbolic computing in Python. *Peer J. Comput. Sci.* 3, e103. doi:10.7717/peerj-cs.103

Möbius, W., Ohno-Iwashita, Y., Van Donselaar, E. G., Oorschot, V. M., Shimada, Y., Fujimoto, T., et al. (2002). Immunoelectron microscopic localization of cholesterol using biotinylated and non-cytolytic perfringolysin O. *J. Histochem. Cytochem.* 50, 43–55. doi:10.1177/002215540205000105

Möbius, W., Van Donselaar, E., Ohno-Iwashita, Y., Shimada, Y., Heijnen, H. F., Slot, J. W., et al. (2003). Recycling compartments and the internal vesicles of multivesicular bodies harbor most of the cholesterol found in the endocytic pathway. *Traffic* 4, 222–231. doi:10.1034/j.1600-0854.2003.00072.x

Naureckiene, S., Sleat, D. E., Lackland, H., Fensom, A., Vanier, M. T., Wattiaux, R., et al. (2000). Identification of HE1 as the second gene of Niemann-Pick C disease. *Science* 290, 2298–2301. doi:10.1126/science.290.5500.2298

Neufeld, E. B., Wastney, M., Patel, S., Suresh, S., Cooney, A. M., Dwyer, N. K., et al. (1999). The Niemann-Pick C1 protein resides in a vesicular compartment linked to retrograde transport of multiple lysosomal cargo. *J. Biol. Chem.* 274, 9627–9635. doi:10.1074/jbc.274.14.9627

Okolo, C. A., Kounatidis, I., Groen, J., Nahas, K. L., Balint, S., Fish, T. M., et al. (2021). Sample preparation strategies for efficient correlation of 3D SIM and soft X-ray tomography data at cryogenic temperatures. *Nat. Protoc.* 16, 2851–2885. doi:10.1038/s41596-021-00522-4

Oninla, V. O., Breiden, B., Babalola, J. O., and Sandhoff, K. (2014). Acid sphingomyelinase activity is regulated by membrane lipids and facilitates cholesterol transfer by NPC2. *J. Lipid Res.* 55, 2606–2619. doi:10.1194/jlr.M054528

Petersen, D., Reinholdt, P., Szomek, M., Hansen, S. K., Poongavanam, V., Dupont, A., et al. (2020). Binding and intracellular transport of 25-hydroxycholesterol by Niemann-Pick C2 protein. *Biochim. Biophys. Acta Biomembr.* 1862, 183063. doi:10.1016/j.bbamem.2019.183063

Petersen, N. H., Faegeman, N. J., Yu, L., and Wustner, D. (2008). Kinetic imaging of NPC1L1 and sterol trafficking between plasma membrane and recycling endosomes in hepatoma cells. *J. Lipid Res.* 49, 2023–2037. doi:10.1194/jlr.M800145-JLR200

Pfeffer, S. R. (2019). NPC intracellular cholesterol transporter 1 (NPC1)-mediated cholesterol export from lysosomes. *J. Biol. Chem.* 294, 1706–1709. doi:10.1074/jbc.TM118.004165

Rosenbaum, A. I., Zhang, G., Warren, J. D., and Maxfield, F. R. (2010). Endocytosis of beta-cyclodextrins is responsible for cholesterol reduction in Niemann-Pick type C mutant cells. *Proc. Natl. Acad. Sci. U. S. A.* 107, 5477–5482. doi:10.1073/pnas.0914309107

Rueden, C. T., Schindelin, J., Hiner, M. C., Dezonia, B. E., Walter, A. E., Arena, E. T., et al. (2017). ImageJ2: ImageJ for the next generation of scientific image data. *BMC Bioinforma.* 18, 529. doi:10.1186/s12859-017-1934-z

Schneider, G., Guttmann, P., Heim, S., Rehbein, S., Mueller, F., Nagashima, K., et al. (2010). Three-dimensional cellular ultrastructure resolved by X-ray microscopy. *Nat. Methods* 7, 985–987. doi:10.1038/nmeth.1533

Schneider, G., Guttmann, P., Rehbein, S., Werner, S., and Follath, R. (2012). Cryo X-ray microscope with flat sample geometry for correlative fluorescence and nanoscale tomographic imaging. *J. Struct. Biol.* 177, 212–223. doi:10.1016/j.jsb.2011.12.023

Settembre, C., Fraldi, A., Medina, D. L., and Ballabio, A. (2013). Signals from the lysosome: a control centre for cellular clearance and energy metabolism. *Nat. Rev. Mol. Cell Biol.* 14, 283–296. doi:10.1038/nrm3565

Sopasakis, P., Sarimveis, H., Macheras, P., and Dokoumetzidis, A. (2018). Fractional calculus in pharmacokinetics. *J. Pharmacokinet. Pharmacodyn.* 45, 107–125. doi:10.1007/s10928-017-9547-8

Stoeck, I. K., Lee, J. Y., Tabata, K., Romero-Brey, I., Paul, D., Schult, P., et al. (2018). Hepatitis C virus replication depends on endosomal cholesterol homeostasis. *J. Virol.* 92, e01196. doi:10.1128/JVI.01196-17

Strauss, K., Goebel, C., Runz, H., Mobius, W., Weiss, S., Feussner, I., et al. (2010). Exosome secretion ameliorates lysosomal storage of cholesterol in Niemann-Pick type C disease. *J. Biol. Chem.* 285, 26279–26288. doi:10.1074/jbc.M110.134775

Trajkovic, K., Hsu, C., Chiantia, S., Rajendran, L., Wenzel, D., Wieland, F., et al. (2008). Ceramide triggers budding of exosome vesicles into multivesicular endosomes. *Science* 319, 1244–1247. doi:10.1126/science.1153124

Vacca, F., Vossio, S., Mercier, V., Moreau, D., Johnson, S., Scott, C. C., et al. (2019). Cyclodextrin triggers MCOLN1-dependent endo-lysosome secretion in Niemann-Pick type C cells. *J. Lipid Res.* 60, 832–843. doi:10.1194/jlr.M089979

Van Der Kant, R., Zondervan, I., Janssen, L., and Neefjes, J. (2013). Cholesterol-binding molecules MLN64 and ORP1L mark distinct late endosomes with transporters ABCA3 and NPC1. *J. Lipid Res.* 54, 2153–2165. doi:10.1194/jlr.M037325

Virtanen, P., Gommers, R., Oliphant, T. E., Haberland, M., Reddy, T., Cournapeau, D., et al. (2020). SciPy 1.0: fundamental algorithms for scientific computing in Python. *Nat. Methods* 17, 261–272. doi:10.1038/s41592-019-0686-2

Wagenmakers, E.-J., and Farrell, S. (2004). AIC model selection using Akaike weights. *Psychon. Bull. Rev.* 11, 192–196. doi:10.3758/bf03206482

Wang, M. L., Motamed, M., Infante, R. E., Abi-Mosleh, L., Kwon, H. J., Brown, M. S., et al. (2010). Identification of surface residues on Niemann-Pick C2 essential for hydrophobic handoff of cholesterol to NPC1 in lysosomes. *Cell Metab.* 12, 166–173. doi:10.1016/j.cmet.2010.05.016

Winkler, M. B. L., Kidmose, R. T., Szomek, M., Thaysen, K., Rawson, S., Muench, S. P., et al. (2019). Structural insight into eukaryotic sterol transport through niemann-pick type C proteins. *Cell* 179, 485–497. doi:10.1016/j.cell.2019.08.038

Wüstner, D. (2005a). Improved visualization and quantitative analysis of fluorescent membrane sterol in polarized hepatic cells. *J. Microsc.* 220, 47–64. doi:10.1111/j.1365-2818.2005.01516.x

Wüstner, D. (2005b). Mathematical analysis of hepatic high density lipoprotein transport based on quantitative imaging data. *J. Biol. Chem.* 280, 6766–6779. doi:10.1074/jbc.M413238200

Wüstner, D. (2006a). Quantification of polarized trafficking of transferrin and comparison with bulk membrane transport in hepatic cells. *Biochem. J.* 400, 267–280. doi:10.1042/BJ20060626

Wüstner, D. (2006b). Steady state analysis and experimental validation of a model for hepatic high density lipoprotein transport. *Traffic* 7, 699–715. doi:10.1111/j.1398-9219.2006.00421.x

Wustner, D. (2019). Steady state analysis of influx and transbilayer distribution of ergosterol in the yeast plasma membrane. *Theor. Biol. Med. Model* 16, 13. doi:10.1186/s12976-019-0108-2

Wüstner, D., Herrmann, A., Hao, M., and Maxfield, F. R. (2002). Rapid nonvesicular transport of sterol between the plasma membrane domains of polarized hepatic cells. *J. Biol. Chem.* 277, 30325–30336. doi:10.1074/jbc.M202626200

Wüstner, D., Mondal, M., Tabas, I., and Maxfield, F. R. (2005). Direct observation of rapid internalization and intracellular transport of sterol by macrophage foam cells. *Traffic* 6, 396–412. doi:10.1111/j.1600-0854.2005.00285.x

Wüstner, D., and Solanko, K. A. (2015). How cholesterol interacts with proteins and lipids during its intracellular transport. *Biochim. Biophys. Acta* 1848, 1908–1926. doi:10.1016/j.bbamem.2015.05.010

Wüstner, D., Solanko, L. M., Lund, F. W., Sage, D., Schroll, J. A., and Lomholt, M. A. (2012). Quantitative fluorescence loss in photobleaching for analysis of protein transport and aggregation. *BMC Bioinforma.* 13, 296. doi:10.1186/1471-2105-13-296

Xu, Z., Farver, W., Kodukula, S., and Storch, J. (2008). Regulation of sterol transport between membranes and NPC2. *Biochemistry* 47, 11134–11143. doi:10.1021/bi801328u